

See discussions, stats, and author profiles for this publication at: <https://www.researchgate.net/publication/263955431>

Pneumatochemical Immittance Spectroscopy for Hydrogen Storage Kinetics

ARTICLE *in* THE JOURNAL OF PHYSICAL CHEMISTRY C · SEPTEMBER 2013

Impact Factor: 4.77 · DOI: 10.1021/jp4023647

CITATION

1

READS

19

6 AUTHORS, INCLUDING:



Eui-Chol Shin

Chonnam National University

22 PUBLICATIONS 102 CITATIONS

[SEE PROFILE](#)



C. N. Park

Chonnam National University

105 PUBLICATIONS 1,387 CITATIONS

[SEE PROFILE](#)



Jong-Sook Lee

Chonnam National University

79 PUBLICATIONS 972 CITATIONS

[SEE PROFILE](#)

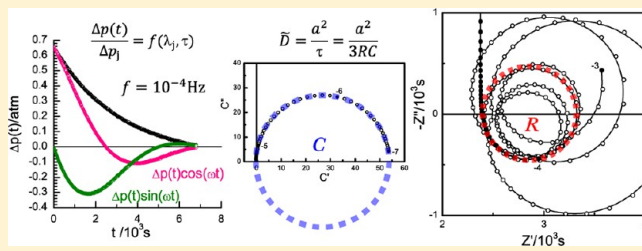
Pneumatochemical Immittance Spectroscopy for Hydrogen Storage Kinetics

Eui-Chol Shin,[†] Young-Hun Kim,[†] Sun-Jung Kim,[‡] Choong-Nyeon Park,[†] Jaekook Kim,[†] and Jong-Sook Lee^{*,†}

[†]School of Materials Science and Engineering, Chonnam National University, Gwangju 500-757, Korea

[‡]Mirae SI Co. Ltd., Gwangju 500-470, Korea

ABSTRACT: Frequency domain analysis of the hydrogen storage kinetics was performed by Fourier transformation of the point relaxation data monitored for a pressure–composition isotherm (PCI) of Mg/MgH₂ system at 325 °C. The correlated hydrogen flux and the pressure relaxation under constant-volume conditions in a typical Sievert's type setup leads to the presence of the characteristic inductive loop, the size of which corresponds to *R* parameter for RC transmission line model for diffusion in the spherical geometry, while the theoretical dc limit resistance may not indicate the diffusion contribution only. The kinetic information was shown equivalent to that of time-domain analysis based on the diffusion problem of a solute in a limited amount into solid state from a well-stirred medium [J. Phys. Chem. C 2013, DOI: 10.1021/jp401286b]. The spectra further develop into the oscillating trajectories originating from the truncation in the sampling. The essential experimental features can be simulated by a RL two-rail transmission line model. A parametric analysis of the preoscillation spectral range using ideal lumped elements provided information on the exponential relaxation constants, nucleation/surface reaction in the two-phase region, and the sampling periods as well as the diffusivity. The pneumatochemical immittance spectroscopy (PnIS) developed in the present work allows a fully automated hydrogen storage kinetic analysis with visualized *R* and *C* parameters for the estimation of chemical diffusivity as a function of storage state using the relaxation data measured for PCI by conventional Sievert's apparatuses.



INTRODUCTION

Hydrogen storage is considered to be the bottleneck to the Hydrogen Economy. For the storage applications, the thermodynamic information on the pressure and the hydrogen amount should be known which is represented by the pressure–composition isotherms (PCI). For the measurement of an isotherm individual relaxations after intermittent hydrogen injection is monitored to a saturation point to obtain the (near) equilibrium values of the pressure as a function of the hydrogen composition.

The relaxation behavior in each point measurement represents the hydrogen storage kinetics for the given state of hydrogen storage amount. Diffusion in the solid state is often the slowest rate-controlling step in the hydrogen storage in unpassivated metal hydrides. A quantitative estimation of chemical diffusivity, \tilde{D} , has been rarely performed for the hydrogen storage, however. A large quantity of the kinetic data are recorded for the measurement of each pressure–composition isotherms (PCI), but they are so far mostly discarded without a further evaluation. In electrochemical storage systems, kinetic analyses on the relaxations upon intermittent potentiostatic/galvanostatic titration steps are well established and widely practiced, which are known as potentiostatic intermittent titration technique (PITT) and galvanostatic intermittent titration technique (GITT).

The immediate problem in the kinetic analysis for the hydrogen storage is the not-straightforward force-flux formulation. In a typical volumetric method using a Sieverts apparatus, the single parameter pressure is monitored, which not only represents the

driving force for the storage but also is converted to the hydrogen absorption amount by the gas law. Pneumatochemical impedance spectroscopy, or PIS, suggested by Millet^{1–5} addressed this issue by designing a special setup where the two pressure signals are monitored for the separation of force and flux term. Neither signals are, however, regulated constant as for the potentiostatic or galvanostatic condition in the electrochemical relaxation measurements. Therefore, Fourier transforms of the two pressure signals are performed to obtain pneumatochemical impedance spectra representing hydrogen storage kinetics. The requirements for special custom-made setup and the data acquisition and processing procedure have so far confined the technique to the work group and their collaboration.^{5–8}

We recently solved the diffusion problem for the pressure relaxations in a typical Sievert's setup.⁹ The boundary condition for the diffusion problem is the supply of a limited amount of hydrogen by the pneumatic control for each point measurement. The hydrogen solute then diffuses into the solid-state storage material with the corresponding decrease in the pressure or concentration in the surrounding medium of a constant volume. The problem is known as the diffusion of a solute in a limited amount from a well-stirred fluid,^{10–12} which can be applied ideally for the sorption of gas or vapors by solids. The effective

Received: March 7, 2013

Revised: July 8, 2013

Published: August 19, 2013

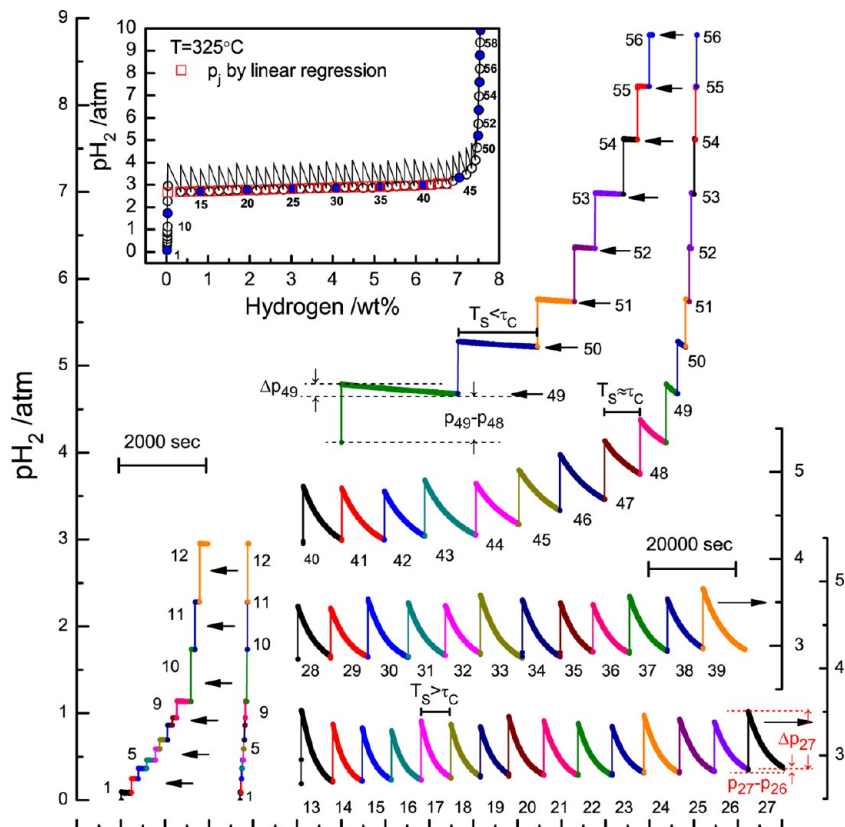


Figure 1. Point relaxations (No. 1 to 56) of the pressure–composition isotherm of Mg/MgH₂ system at 325 °C shown in the inset. The plateau region is smoothed by a linear regression. Each relaxation is preceded by the pressure regulation step outside the chamber (not shown). The arrows indicate the magnified plots by a factor of ten in the time scale.

volume ratio λ parameter in the diffusion equation characterizes the relaxation behavior. The parameter is determined by the hydrogen absorption amount and the equilibrium pressure and thus the thermodynamic information already evaluated for PCI. The plateau region corresponds to the λ value approaching zero, while $\lambda = \infty$ limit corresponds to the well-known constant pressure or constant surface activity. The application of the diffusion solution for different λ values allows the evaluation of diffusion coefficients as a function of state of storage (SoS) in a close analogy to the intermittent titration techniques in electrochemistry.^{13–15} It is named as pneumatochemical intermittent titration technique, or PnITT.⁹

On the basis of the understanding on the time-domain response of the relaxation curves, this work reports on the frequency-domain analysis by Fourier transformation. Pneumatochemical impedance is derived from the single pressure signal by the conventional Sievert's method turns out quite distinct from PIS results by Millet et al.^{1–5} from the two separately monitored pressure signals. Very intriguing and nontrivial spectral feature is largely explained, which is supported by the deconvoluted kinetic information that is shown equivalent to that by the time domain analysis. The frequency domain method also allows a full automatic kinetic analysis.

■ EXPERIMENTAL SECTION

The same experimental relaxation data for the time-domain analysis⁹ are used. Commercial MgH₂ powder (Alfa Aesar, 98% balance Mg) was used for the experiments. The pressure–composition–temperature (PCT) analysis (Anyisorb HQ, Mirae SI, Korea) was performed using 1 g of MgH₂ powder. The sample

was pretreated at 450 °C for 2 h. The hydrogenation was performed at 325 °C by intermittent hydrogen injection about 91 h for the pressure–composition isotherm with 64 point relaxations. The measurement procedure with data recording is fully automated. Further details of the experiments and the structural and thermal characteristics of the MgH₂ powders can be found elsewhere.⁹ Numerical Fourier transformation was performed using commercial spreadsheet software of MS Excel 2010 with Visual Basics for Applications (VBA). Impedance simulation and analysis were performed by Zview (Scribner Ass. USA),¹⁶ MEISP (Kumho Petrochemical Co., Korea),¹⁷ and Matlab (Mathworks, USA).

■ THEORETICAL CONSIDERATIONS

Time-Domain Analysis. The time-domain analysis of the point relaxation data for chemical diffusivity and hydrogen diffusivity has been recently performed for the first time.⁹ The essential aspects necessary for the present work will be briefly introduced. The measurement of an isotherm shown in the inset of Figure 1 is constituted by a series of relaxation experiments after hydrogen injection until (near) equilibrium value p_j is reached. In the typical Sievert's setup, hydrogen stored in the reference chamber is injected to the sample chamber by the mechanical valve action as previously illustrated.⁹ The boundary condition for the diffusion equation is represented by λ parameter, which is the ratio $(p_j - p_{j-1})/\Delta p_j$. The p_j and Δp_j are indicated for the points 27 and 49 in Figure 1. As Δp_j represents the hydrogen absorption amount in the constant volume condition, λ values correspond to the local slopes of the pressure–composition curve.

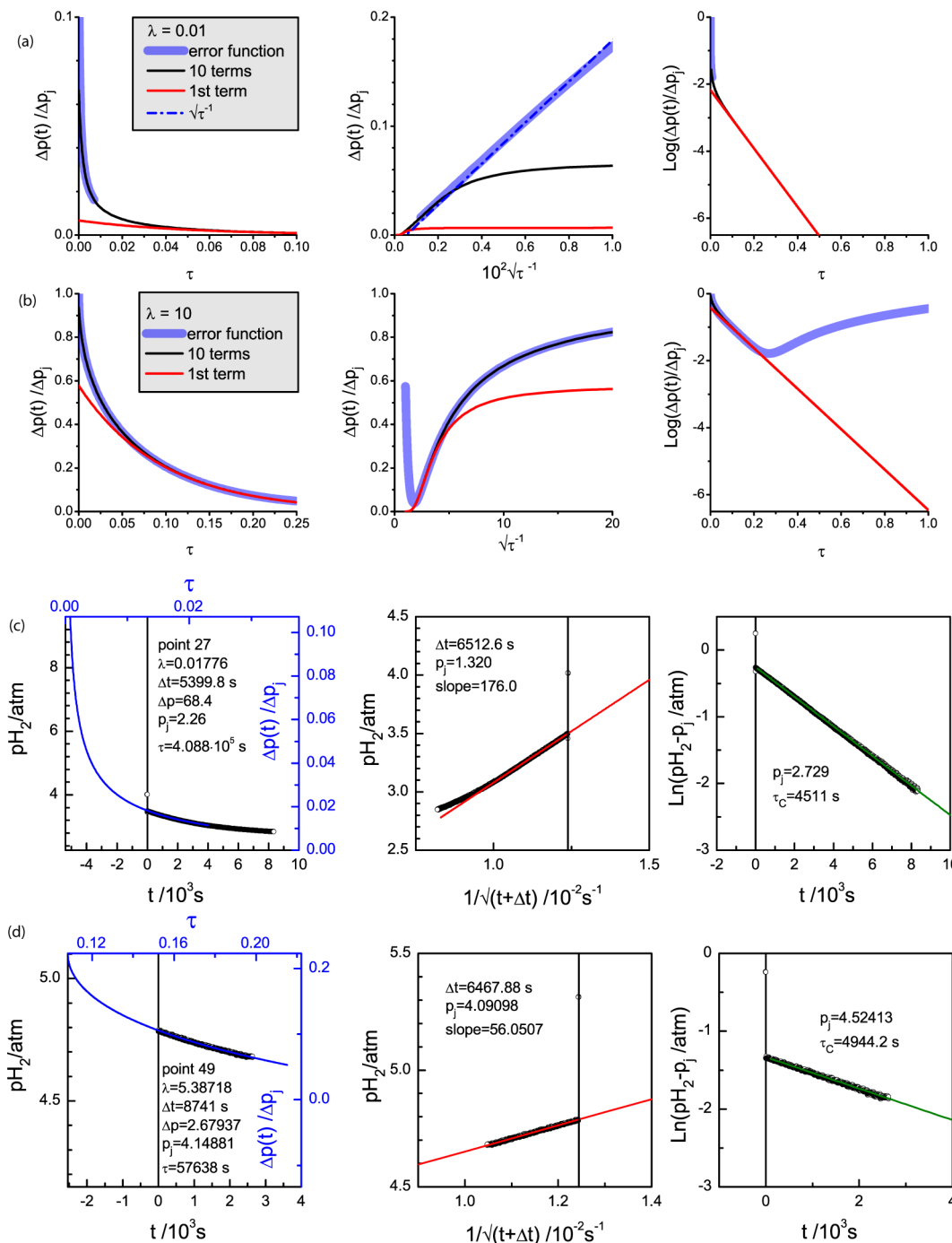


Figure 2. Pressure relaxation simulations according to eq 3 (blue), summation from $n = 1$ to 10 (black), and $n = 1$ term (red) in Figure 1 in various scales for $\lambda = 0.01$ (a) and 10 (b). Fit results of experimental relaxation curve of point 27 with $\lambda = 0.018$ (c) and point 49 with $\lambda = 5.39$ (d) in various representations.

The diffusion of a limited amount of hydrogen into the solid state storage material particle with the radius a from the well-stirred (homogeneous) gas medium can be given by the series of the exponential function term with parameter λ as^{10–12}

$$\frac{\Delta p(t)}{\Delta p_j} = \sum_{n=1}^{\infty} \frac{6\lambda(1+\lambda)}{9(1+\lambda) + \lambda^2 q_n^2} \exp(-q_n^2 \tau) \quad (1)$$

where $\tau = \tilde{D}t/a^2$, q_n are nonzero, positive roots of

$$\tan q = \frac{3q}{3 + \lambda q^2} \quad (2)$$

Figure 2a,b illustrates the typical behavior of small and large λ values as a function of the normalized time $\tau = \tilde{D}t/a^2$. For $\lambda = 10$, the first term of eq 1 is sufficient for the description of the relaxation for $\tau > 0.1$. The limiting case of $\lambda = \infty$ corresponds to the constant pressure condition. For $\lambda = 0.01$, $\Delta p(t)/\Delta p_j$ instantaneously drops below 10%. As indicated in the logarithmic plot, the first term approximation is of little practical use since $\Delta p(t)/\Delta p_j$ becomes below less than 0.1% for $\tau \gtrsim 0.1$. Note that τ is the normalized time as $\tau = \tilde{D}t/a^2$. Small λ value represents the absorption of the limited amount of solute into a large capacity sorbent so the relaxation completes much faster than supposed

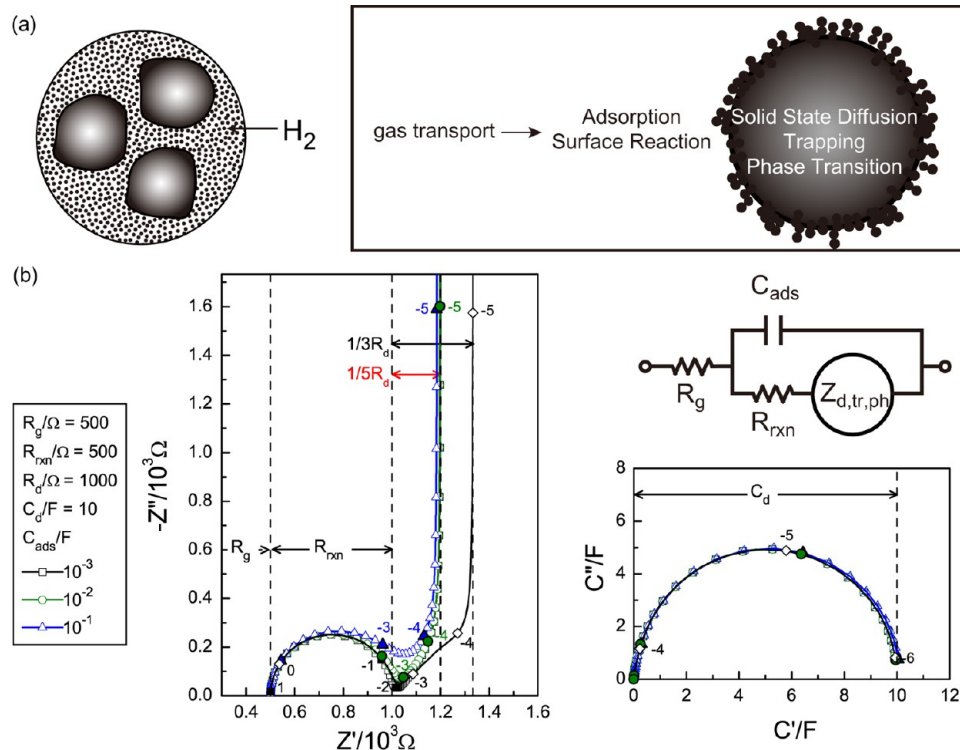


Figure 3. (a) Hydrogen storage in the particulates (left) can be modeled as the mass transport in a sphere of average size (right). (b) Pneumatochemical impedance model in analogy to the electrochemical impedance where R_g is gas phase transport, R_{rxn} and C_{ads} are for surface reaction, and $Z_{d,tr,ph}$ is for the storage process in the solid state. The impedance and complex capacitance spectra for different adsorption capacitances in comparison with diffusion in the planar geometry. The numbers are logarithmic frequencies.

for the constant pressure case with the same chemical diffusivity. Since λ corresponds to the thermodynamic factor or inverse chemical capacitance, small λ reduces the chemical diffusivity, but the depression of the apparent hydrogen storage kinetics become less prominent.

The thick blue lines in Figure 2a,b shows that the relaxation behavior can be satisfactorily described by the first term ($n = 1$) of the (complementary) error function solution in spherical geometry as^{10–12}

$$\frac{\Delta p(t)}{\Delta p_j} = (1 + \lambda) \left[\frac{\gamma_1}{\gamma_1 + \gamma_2} e \operatorname{erfc} \frac{3\gamma_1}{\lambda} \sqrt{\tau} + \frac{\gamma_2}{\gamma_1 + \gamma_2} e \operatorname{erfc} \left(-\frac{3\gamma_2}{\lambda} \sqrt{\tau} + \text{higher terms} \right) \right] - \lambda \quad (3)$$

where

$$\gamma_1 = \frac{1}{2} \left(\sqrt{1 + \frac{4}{3}\lambda} + 1 \right), \quad \gamma_2 = \gamma_1 - 1 \quad (4)$$

and

$$e \operatorname{erfc} z \equiv \exp z^2 \operatorname{erfc} z \quad (5)$$

even for the large λ case. For small λ values, the $\sqrt{\tau}^{-1}$ approximation of the error function solution can be used for not too small τ range.⁹

Figure 2c,d shows the examples of the time-domain analysis for a small and large λ case, respectively. A substantial cutoff in the initial response, Δt , was required. Although all relaxations exhibit an exponential decay, the correct τ value consistent with the error function analysis can be obtained by $\sqrt{\tau}^{-1}$ approximation

for small λ and by the exponential function for large λ , respectively. The technique allows the determination of the chemical diffusivity as a function of state of hydrogen storage varied by consecutive hydrogen injections, similar as the intermittent titration techniques for the electrochemical storage system. The technique has been thus named as pneumatochemical intermittent titration technique (PnITT).⁹

Diffusion Impedance. The frequency domain response, which is in principle equivalent to the time-domain response, can be more powerful in the deconvolution of multiscale responses. As well as suggested for hydrogen storage kinetic analysis by Millet et al.,^{1–5} Boukamp et al.¹⁸ performed a frequency domain analysis of the oxidation kinetics in mixed ionic–electronic conductors by Fourier transform of the conductivity relaxations (CR), which not only provides a more reliable parameter evaluation but also a visual presentation of the limitations and complications of the CR experiments.

As schematically illustrated in Figure 3, top, the hydrogen storage or in general any gas incorporation processes are represented by the multiscale frequency response of the gas phase transport (R_g), surface reaction and adsorption (R_{rxn} and C_{ads}), and often the slowest rate-controlling processes in the solid such as chemical diffusion, trapping, and phase transformation (represented by $Z_{d,tr,ph}$ element) in a close analogy to the electrochemical storage process. Millet and Dantzer developed impedance models for the phase transformation limited by various nucleation and growth process.¹⁹ The simplest case of the one-dimensional phase transformation has been modeled as an RC series circuit.^{19–22} The simple RC series circuit also represents the charge carrier trapping processes.^{23–26} The model has been applied to the ion intercalation processes.^{25,27–29} Trapping of ions can be considered as incipient phase transformation.

Bisquert et al.^{24–27} and Barsoukov et al. combined the trapping or phase transformation^{20–22} in the transmission line model for diffusion processes, one-dimensional diffusion and diffusion in the spherical geometry, respectively. It should be noted that diffusion in spherical geometry can be more appropriate for the practical electrochemical storage system with the particulate material.^{20–22} The diffusion controlled bulk process in planar geometry in close analogy with the electrochemical storage in planar, thin film, and electrodes is described by the well-known Warburg impedance, which is represented by RC transmission line model in finite length with open terminus, Figure 4a. With R_d

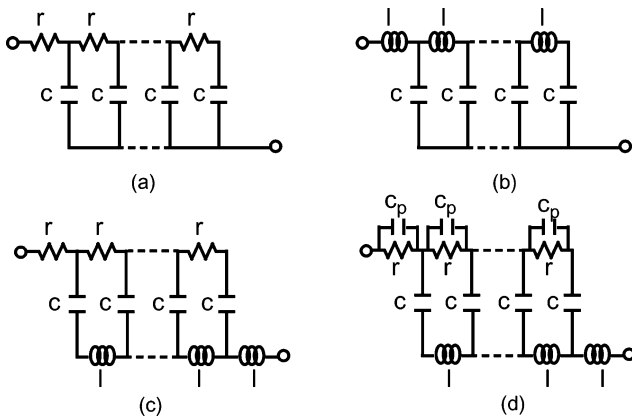


Figure 4. (a) RC transmission line model for finite length diffusion. (b) LC resonance transmission line model. (c) RL two-rail transmission line model for pneumatochemical impedance. (d) Parallel capacitors to the resistor rail for high frequency shunt effects.

and C_d defined as the total resistance and capacitance of the distributed resistors and capacitors in the transmission line model as $R_d = nr$ and $C_d = nc$, the diffusion impedance can be represented as

$$Z_d(\omega) = \sqrt{\frac{R_d}{j\omega C_d}} \coth \sqrt{R_d j\omega C_d} \quad (6)$$

where the chemical diffusivity can be evaluated from the transmission line elements as $\tilde{D} = (L/2)^2/(R_d C_d)$. The low frequency limit resistance and capacitance are $1/3R_d$ and C_d , respectively, as indicated in Figure 3. The impedance plot indicates clearly the slope-one high-frequency region. The capacitance representation of Z_d impedance alone becomes mathematically equivalent to the impedance of finite-length Warburg model with closed terminal. Both presentations have been shown for the transmission-line-like conducting network in dielectric matrix.³⁰ Additional high frequency components in Figure 3 smear out the high frequency Warburg character in the complex capacitance plot in Figure 3.

As also suggested by Millet et al.,^{1–8} the diffusion in the spherical geometry should be considered for the hydrogen storage processes in the particulate material. Impedance for the spherical diffusion can be represented in terms of the transmission line elements as^{22,31}

$$Z_d(\omega) = \frac{\tanh(\sqrt{R_d j\omega(3C_d)})}{\sqrt{\frac{j\omega(3C_d)}{R_d}} - \frac{1}{R_d} \tanh(\sqrt{R_d j\omega(3C_d)})} \quad (7)$$

which defines consistently $\tilde{D} = a^2/(R_d(3C_d))$ as in the one-dimensional case, eq 6. As indicated in Figure 3 the low frequency limit resistance and capacitance, $1/5R_d$ and $((1/3)3)C_d = C_d$,

respectively, are smaller than for the one-dimensional case. The characteristic slope-one Warburg behavior becomes less prominent and easily smeared out by slightly overlapped high frequency response. Moreover, the diffusion process can be extremely non-ideal and thus described by the fractional diffusion equation.^{27,32,33}

Pneumatochemical Inductance. Warburg diffusion impedance eqs 6 and 7 can be straightforwardly derived from the Laplace transform of the diffusion equation under constant potential or concentration condition.^{11–13,29,31} The slope-one high frequency behavior and capacitive behavior at low frequency corresponds to the time-domain response of the current proportional to $\sqrt{t^{-1}}$ in the short-time limit and the exponential decay in the long time limit,^{13–15} or by integrating the concentration varies as $- \sqrt{t}$ at short times and exponentially at long times.⁹ However, for small λ as shown in Figure 2a the \sqrt{t} dependence is practically unobservable.⁹ The initial drop, e.g., to 10% of the (theoretical) full Δp_i occurs immediately.⁹ Most of the relaxation is described by the short-time error function solution or $\sqrt{t^{-1}}$ dependence, rather than \sqrt{t} dependence, distinctly different from the constant surface activity condition. The control parameter also becomes a pulse-like rather than a step function.⁹

Laplace transformation of the diffusion solution in a solid in contact with well-stirred fluid is far more involved than for the boundary condition of constant surface concentration.¹² The same response function should be obtained regardless of the types of the trigger function in the linear system. There is a more fundamental difficulty in the evaluation of pneumatochemical impedance from the pressure response by the volumetric method, however. The parameter pressure not only represents the driving force for the storage but also directly indicates the hydrogen absorption amount by the gas law. The PIS technique developed by Millet et al.^{1–5} tackled this issue by monitoring the two pressure parameters for the driving force and the flux, but the method is in principle a volumetric one and the force-flux correlation issue still exists.

We suggest that the force-flux correlation leads to the inductor-related response in the pneumatochemical impedance derived from the pressure relaxation using a Sievert's setup. The force and flux term bear a unique relationship in the gas phase absorption under constant volume conditions

$$i(t) = -dp(t)/dt \quad (8)$$

i.e., the hydrogen flux is proportional to the time derivative of the pressure, which is the formal driving force. In eq 8, the pressure-volume conversion factor determined by the chamber volume and the gas law is set to unity for simplicity. The essence can be illustrated by the diagram in Figure 5 where a storage material

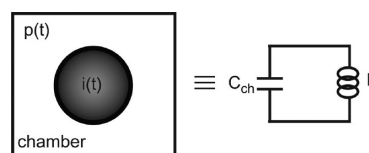


Figure 5. Constant volume chamber with hydrogen storage material working as an inductor in the electrical circuit.

with the flux $i(t)$ is located in a chamber with pressure $p(t)$. Since $i(t) = -i_{ch}(t)$, the relationship represents the electrical analog of the chamber capacitor $C_{ch} = (Idt)/dV$ as

$$i_{ch}(t) = (C_{ch})(dp(t)/dt) \quad (9)$$

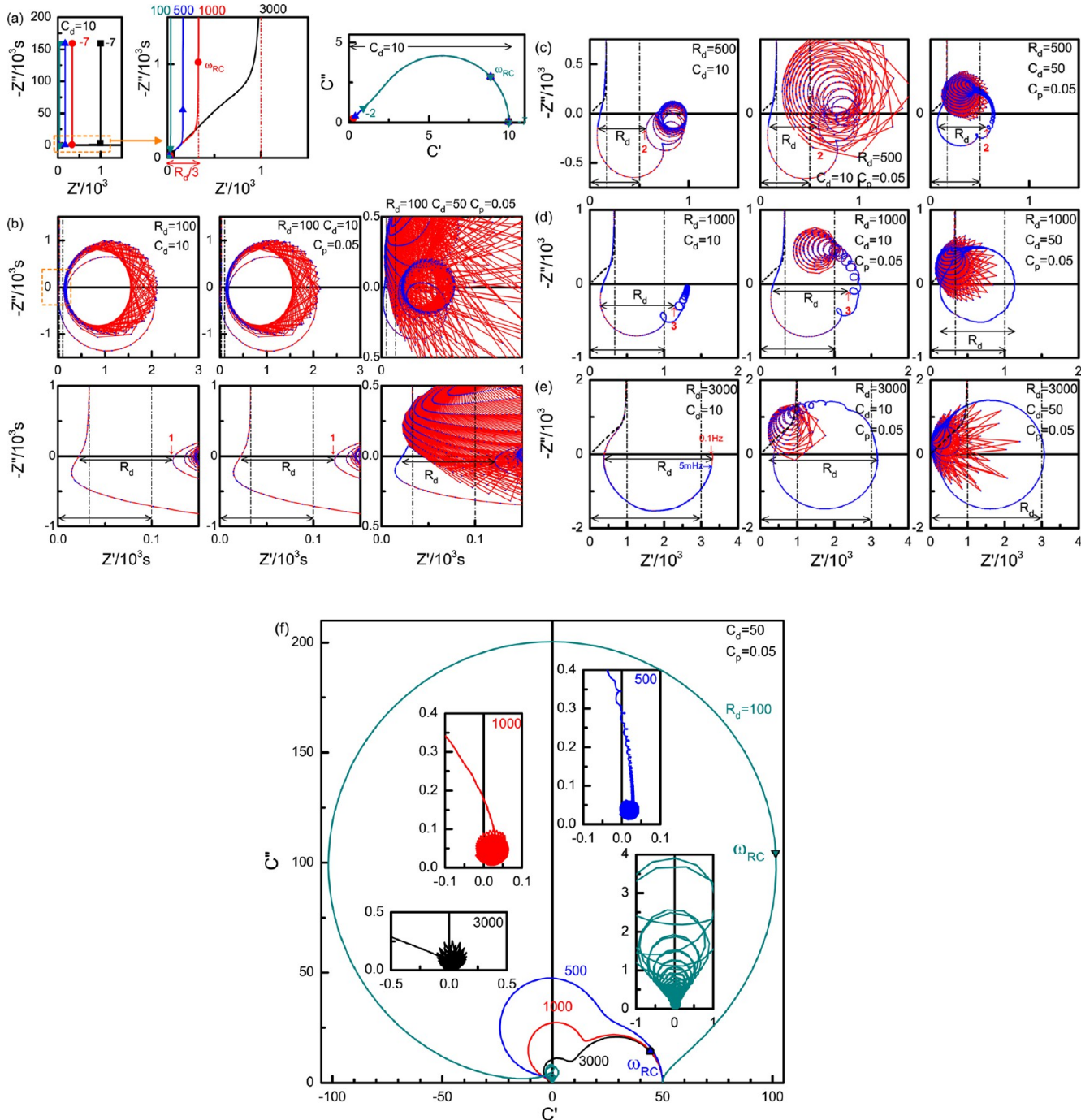


Figure 6. (a) Impedance and capacitance plots of RC transmission line model with $R_d = 100, 500, 1000$, and 3000 (Figure 4a) from 10^{-7} to 10^{-2} Hz. The low magnification plot shown for $f \geq 10^{-7}$ Hz (left) is not isotropic. ω_{RC} indicates the frequency $(R_d C_d)^{-1}$. The low frequency limiting resistance is $R_d/3$. The response of RL two-rail transmission line model (Figure 4c) with $L = 10^6$ is shown in panels b–e in the first column for $10^{-5} \text{ Hz} \lesssim f \leq 10^{-3}$ Hz. The effect of parallel capacitor with $C_p = 0.05$ to resistor elements is shown in the second column graph of panels b–e. The third column graphs of panels b–e represent the impedance with $C_d = 50$. (f) Complex capacitance plots for $L = 10^6$, $C_d = 50$, $C_p = 0.05$, and $R_d = 500, 1000$, and 3000 corresponding to the third column graphs of panels b–e.

Let us assume the storage material behaves an ideal pneumatochemical inductor, L , without the storage capacity (C) or loss (R), which can be defined in analogy to the electricity as

$$p(t) = L(d\dot{i}/dt) \quad (10)$$

where $p(t)$ represents back- or counter-pressure from the inductor to the chamber. Then, eqs 8 and 9 result in the differential equation

$$i(t) = -L d^2 i(t)/dt^2 \quad (11)$$

and thus, as well known in LC circuit theory, when the chamber is first pressurized and closed, an oscillating hydrogen flux $i(t)$ with resonance frequency $f = (2\pi(LC_{ch})^{1/2})^{-1}$ can be developed as

$$i(t) \propto e^{jt/\sqrt{LC_{ch}}} \quad (12)$$

where $C_{ch} = 1$ is defined by eq 9. Therefore, the force–flux relationship in the hydrogen storage kinetics leads to an pneumatochemical analog of an electrical inductor.

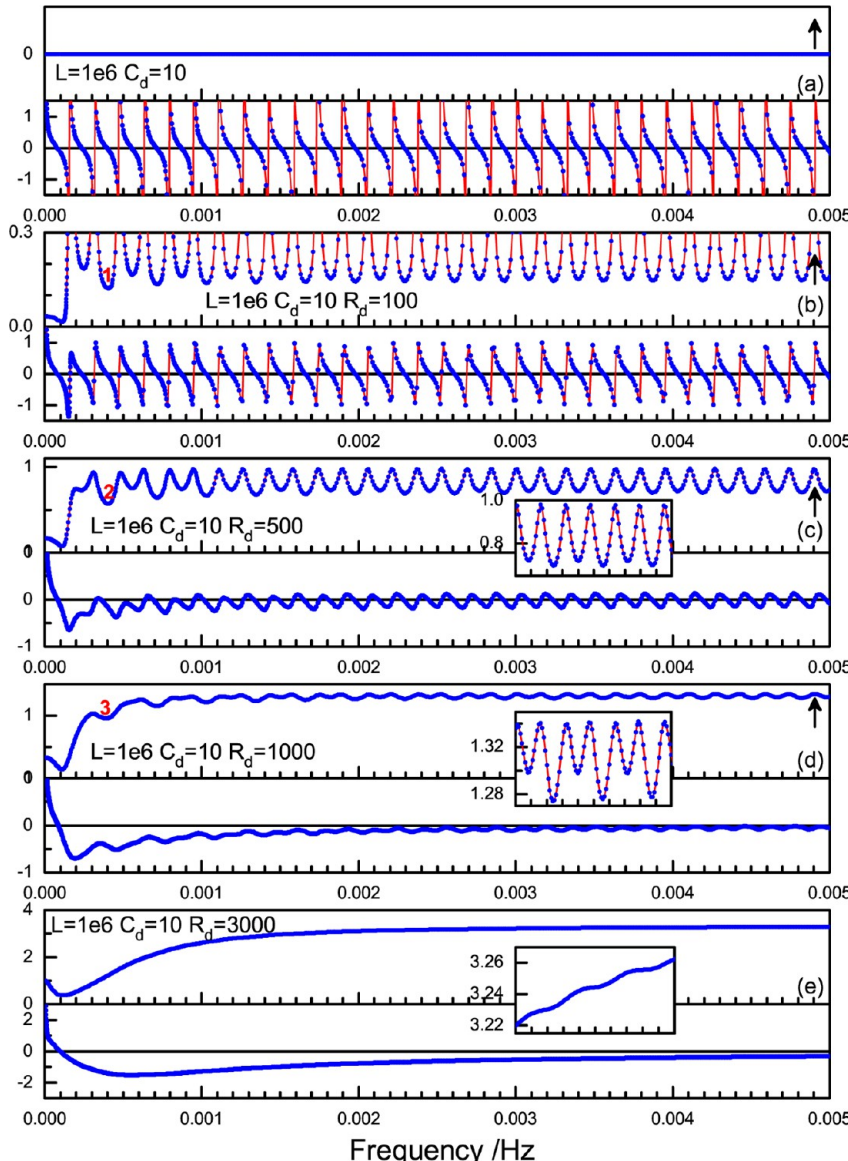


Figure 7. Z' and Z'' in 10^3 as a function of frequencies $f \leq 5$ mHz in linear sweep for an RL two-rail transmission line model with $L = 10^6$ and $C_d = 10$ without R_d rail (Figure 4b) and with $R_d = 100$ (b), 500 (c), 1000 (d), and 3000 (e) (Figure 4c). The insets show the magnified view of Z' for $3 \text{ mHz} \leq f \leq 4 \text{ mHz}$.

Indeed, experimentally evaluated pneumatochemical impedance presented in the next section exhibits characteristic oscillations at constant frequency intervals indefinitely. In the previous section, the hydrogen storage material is modeled as a RC transmission line model for the solid state diffusion process. After testing several possibilities the inductive nature in the hydrogen storage kinetics is included as an additional inductor rail of the total series inductor L as shown in Figure 4c for one-dimensional diffusion. The construction of the circuit assumes to satisfy the Kirchhoff's circuit law, i.e., the total hydrogen flux in the material is the summation of the inductive flux and diffusion or hopping flux

$$i = i_L(x) + i_R(x) \quad (13)$$

and the storage in the capacitor C_d in the transverse direction occurs by the difference in the pressure attenuation between two fluxes, $p_L(x) - p_R(x)$.

It should be noted that the suggested RL two-rail transmission line model is different from the standard transmission line model

described by Telegrapher's equation where the impedance rail along the propagation direction consists of resistors r and inductors l in series in the same rail. Strong impedance oscillation can also occur for the standard transmission line model, but not much has been discussed since the resonant bandwidth is not of practical interest.³⁴

Figures 6–8 are simulations of the transmission line models with parameters comparable to the experimental results presented in the next section. The units for pneumatochemical immittance, not indicated, can be self-consistently and arbitrarily defined. The impedance and capacitance plane presentations of the reference RC transmission line model are shown in Figure 6a for $C_d = 10$ and different $R_d = 100, 500, 1000$, and 3000, respectively, according to eq 6. The first graph of Figure 6a presents the capacitor-dominated impedance response for $f \geq 10^{-7}$ Hz since $Z'' \approx (j\omega C_d)^{-1}$. The low frequency region of the spectrum can be approximated by the series network of $R_d/3$ and C_d as also shown in Figure 3. The high frequency region shows the slope-one Warburg response. Since $C^* = (j\omega Z^*)^{-1}$, the capacitance plots in

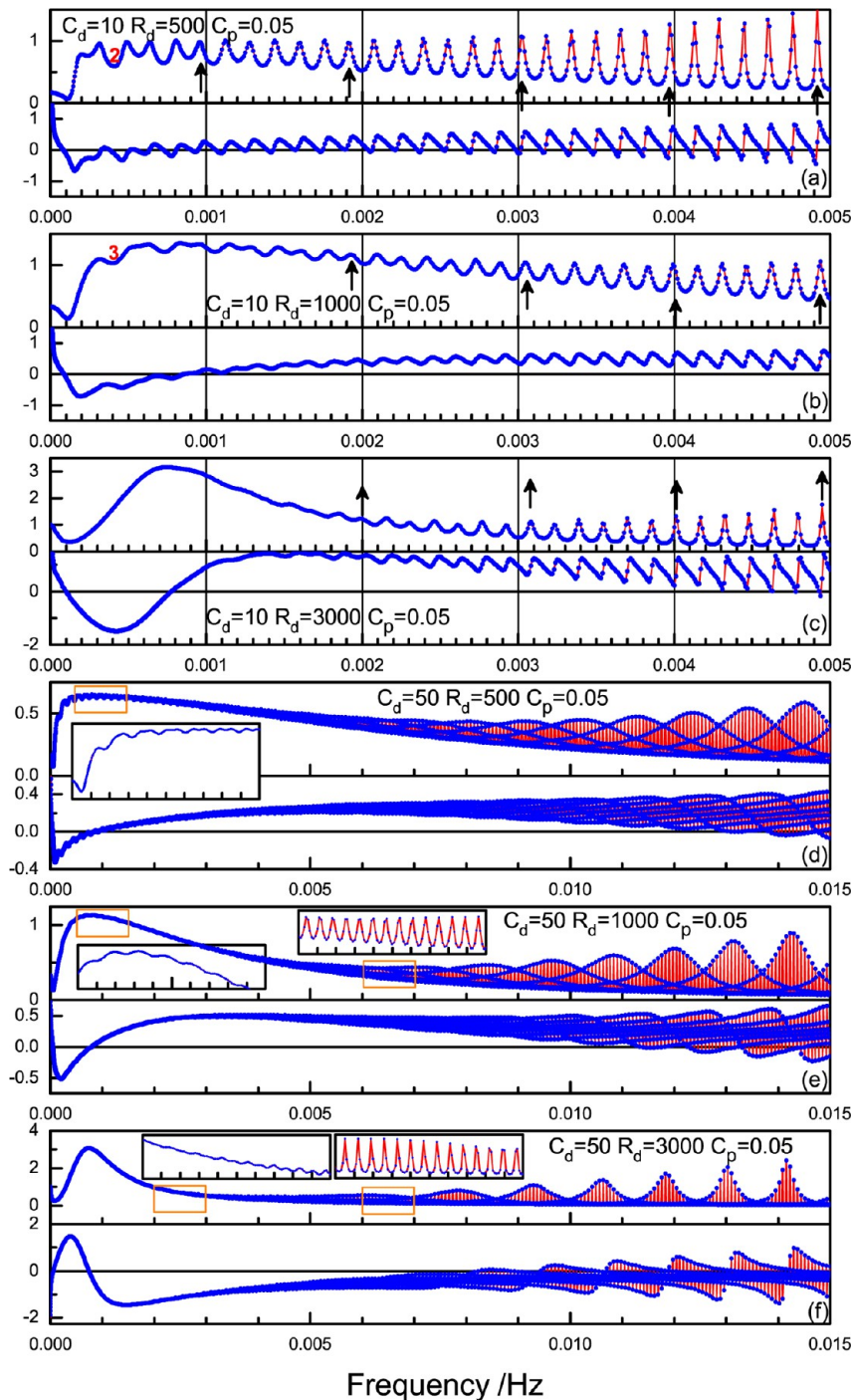


Figure 8. Z' and Z'' in 10^3 as a function of frequencies $f \leq 5$ mHz in linear sweep for an RL two-rail transmission line model with $L = 10^6$, $C_d = 10$, and $C_p = 0.05$ for $R_d = 500$ (a), 1000 (b), and 3000 (c), and as a function of frequencies $f \leq 15$ mHz with $C_d = 50$ for $R_d = 500$ (d), 1000 (e), and 3000 (f). See text for more explanation.

the rightmost graph assume the expression of Warburg impedance with the closed terminal, i.e.

$$C^*(\omega) = \sqrt{\frac{C_d}{j\omega R_d}} \tanh \sqrt{R_d j\omega C_d} \quad (14)$$

The plots present the slope-one high frequency region, which is smeared in Figure 3 due to the additional high frequency responses.

The response of the LC transmission model in Figure 4b is a purely imaginative oscillation as shown in Figure 7a. With $L = 10^6$

and $C_d = 10$, Z'' diverges at frequencies equal to multiples of $(2(LC)^{1/2})^{-1}$, 0.158 mHz. Figure 7b–e shows that the addition of R rail damps the oscillation and doubles the periodicity. The valley depth changes in every other oscillation. See the magnified insets for $3 \text{ mHz} \leq f \leq 4 \text{ mHz}$ in Figure 7c,d. The difference in the valley depth becomes larger with resistance, and eventually the shallow valley becomes a broad hill and the deep second valley becomes a broad valley, as shown in Figure 7e for $R_d = 3000$.

While RC transmission line model presents its R component by $R/3$ dc limit, the RL two-rail transmission line model indicates

R component by the difference in Z' between the first minimum and the next deep valley points as indicated by 1, 2, and 3 in Figure 7b–d, respectively. For not too large R , they mark almost exactly the magnitude of the resistance value R_d of the transmission line model in the impedance plane plots as indicated in Figure 6b–d, first column. For high resistance values such as 3000, shown in Figure 6e, resonance effects appear overshadowed by the formation of the semicircular profile of the diameter R_d , which closes on the Z' axis for $f \lesssim 0.1$ Hz. Hydrogen storage kinetics limited by solid-state diffusion is expected to be described by RL two-rail transmission line model with not-too-small resistance values. The semicircular trajectory at the high frequency region can be described by LR parallel circuit where the fitted R and L parameters are close to the transmission line parameter. L is smaller by ca. 10% and R larger by ca. 3% than R_d . It is thus possible to read out the R_d value graphically from the high frequency inductive loop behavior as well as from the dc limit $R_d/3$ (or $R_d/5$ in spherical diffusion). The dc limit, however, may include the additional response, and the deconvolution may not be easy as already discussed in Figure 3. The inductive effects would make the spectral feature further nontrivial.

Experimental spectra, as will be presented in the next section, indeed exhibit the LR loops, but they make complete circular trajectories, which eventually reduce to the origin. The essential feature can be produced by introducing a parallel capacitor element C_p to resistor element r in the transmission line model, Figure 4d, and the simulations with $C_p = 0.05$ are shown in Figure 8a–c, Z' and Z'' vs frequency, and complex plane representation in the second column of Figure 6c–e, second column. For $R_d = 3000$, an almost complete circular trace with size R_d results. The presence of C_p leads to apparent irregularity in the oscillation interval as indicated by the arrows in Figure 8a–c, which increases with R_d values. This may be attributed to the superposition of the attenuation effect due to C_p and the intrinsic LC oscillations.

Figure 8d,e represents the simulation with $C_d = 50$ increased from Figure 10. Secondary profiles of the resonance peaks are generated. These peak traces are also indicated in the impedance spectra of the third column of Figure 6c,d. Increased C_d decreased the fundamental oscillation by the factor $\sqrt{5}^{-1}$. Increasing C_d relative to the fixed L value strengthened the RC transmission response; thus, the high-frequency slope-one response becomes more visible. The inductive loop starts much closer to the origin, and the circular loop is shifted while the diameter represents more exactly R_d . The variation of the parameters confirms the geometric assessment of R_d by the circular trajectories in the impedance plane.

Figure 6f displays the capacitance plane representations of RL two-rail transmission line models. The semicircular inductive loops in the impedance plane is represented by the additional circular bump at high frequency region where $C' < 0$, which dominates the response for small R_d . As discussed above, for large R_d and C_d the original RC transmission line behavior can be seen at low frequency range and the size of the semicircular response or the low frequency limit indicates C_d . Therefore, both capacitance and impedance representation can be employed for the direct graphical evaluation of R_d and C_d for the hydrogen storage kinetics. The technique developed in the present work is named as pneumatochemical immittance spectroscopy, or PnIS, where the immittance³⁵ emphasizes the exploitation of different response functions. The name also serves the purpose of distinction from PIS suggested by Millet et al.^{3–5}

RESULTS AND DISCUSSION

Numerical Data Processing. Our recent accomplishment in the time-domain analysis of the point relaxation curves⁹ allows in-depth understanding of the frequency-domain response of the relaxation data. As suggested by Millet et al.^{1–5} and Boukamp et al.¹⁸ the frequency domain analysis can be a more powerful tool for kinetic analysis. The parametric analysis for multiscale responses can be much more easily performed with the frequency response, generally measured logarithmically over decades.

The pneumatochemical impedance is defined as $Z_{pn}(\omega) = p(\omega)/i(\omega)$, where $p(\omega)$ and $i(\omega)$ are the Fourier transformation of the pressure $p(t)$ as the driving force and the hydrogen flow $i(t)$, respectively. By the constant-volume conditions and the gas law, the hydrogen flux can be represented by the time variation of the pressure. The pneumatochemical impedance thus defined in unit of seconds in the present work as

$$Z_{pn} = \frac{p(\omega)}{i(\omega)} = \frac{p(\omega)}{-(dp/dt)(\omega)} \quad (15)$$

The pneumatochemical impedance is evaluated from experimental relaxation curves $p(t)$ for Mg/MgH₂ system at 325 °C shown in Figure 1. For the evaluation of $p(\omega)$, not only the relaxation $\Delta p(t)$ but the step-function contribution from the equilibrium pressure of the previous point measurement, $p_j - p_{j-1}$, should be considered, viz.

$$p(\omega) = \int_0^\infty \Delta p(t) \exp(-j\omega t) dt + \frac{p_j - p_{j-1}}{j\omega} \quad (16)$$

The p_j values in the plateau region should increase with hydrogen absorption but experimental measurements exhibit fluctuations as the variation in p_j is small. A linear regression was performed so that $(p_j - p_{j-1}) > 0$, and thus $\lambda_j = (p_j - p_{j-1})/\Delta p_j > 0$ to satisfy the causality relationship. The correlated change in the evaluation of Δp_j for the hydrogen absorption amount is minor and thus neglected.

Since the hydrogen absorption amount is proportional to the pressure change, (dp/dt) is the same as $(d\Delta p(t)/dt)$. The Fourier transform of the differential function, $d\Delta p(t)/dt$, can be represented in terms of the Fourier transform of $\Delta p(t)$ as

$$(d\Delta p(t)/dt)(\omega) = j\omega \int_0^\infty \Delta p(t) \exp(-j\omega t) dt - \Delta p_j \quad (17)$$

Thus, the pneumatochemical impedance of eq 15 can be evaluated as

$$Z_{pn}(\omega) = \frac{\int_0^\infty \Delta p(t) e^{-j\omega t} dt + (p_j - p_{j-1})/j\omega}{\Delta p_j - j\omega \int_0^\infty \Delta p(t) e^{-j\omega t} dt} \quad (18)$$

using the Fourier transformation of $\Delta p(t)$, $\Delta p(\omega) = \int_0^\infty \Delta p(t) e^{-j\omega t} dt$ only. Δp_j and p_j are constants obtained from the relaxation data in Figure 1. There is no need to obtain $(dp\Delta(t)/dt)$ by differentiation of $\Delta p(t)$ and then $i(\omega)$ by the Fourier transform. The limited digitization resolution in the experimental $p(t)$ would not allow numerical differentiation of the raw data easily.

The integral term can be evaluated numerically by summation of $\Delta p(t) \cos(\omega t)$ and $\Delta p(t) \sin(\omega t)$ as shown in Figure 9 for an arbitrarily selected frequency. The standard trapezoidal numerical integration was performed using a visual basic spreadsheet macro in Excel, similarly as in the previous work.^{36,37} For the given frequency, the exact same results are obtained by the fast

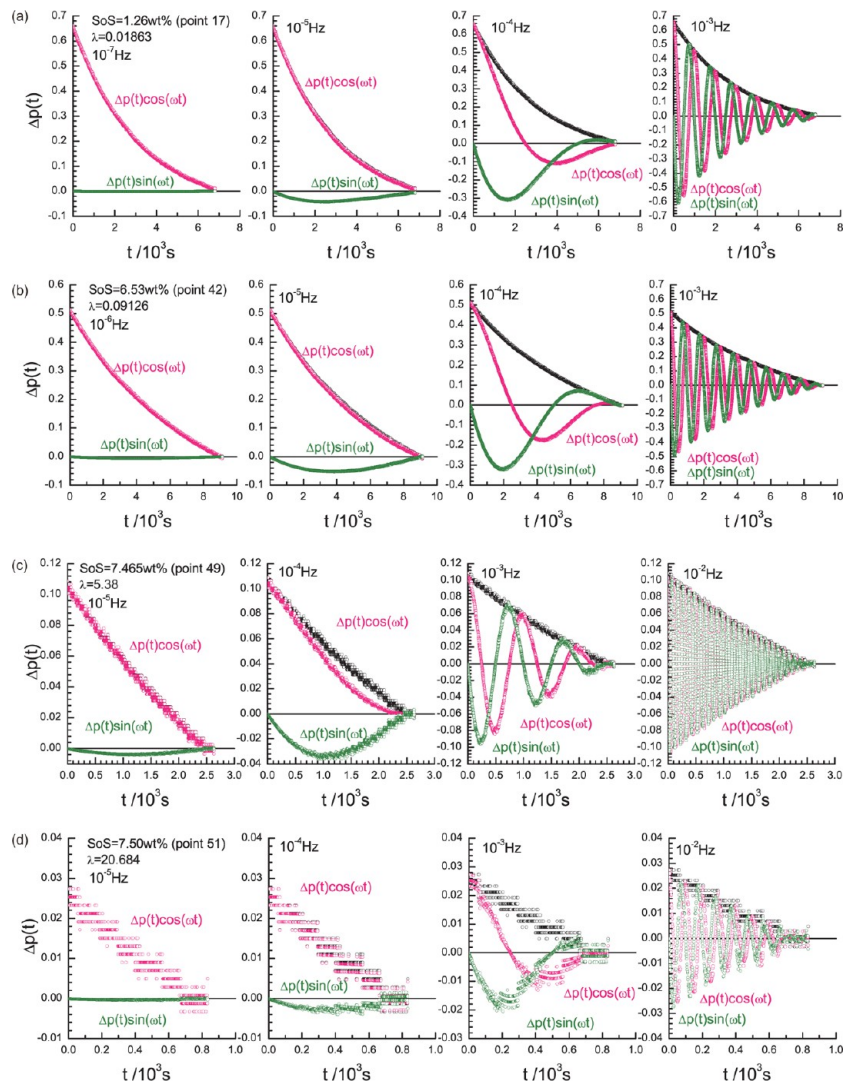


Figure 9. Numerical integration of $\Delta p(t) e^{-j\omega t}$ term for Z_{Pn} calculation for selected points at different states of storage. Points 17, 42, 49, and 51 in Figure 1.

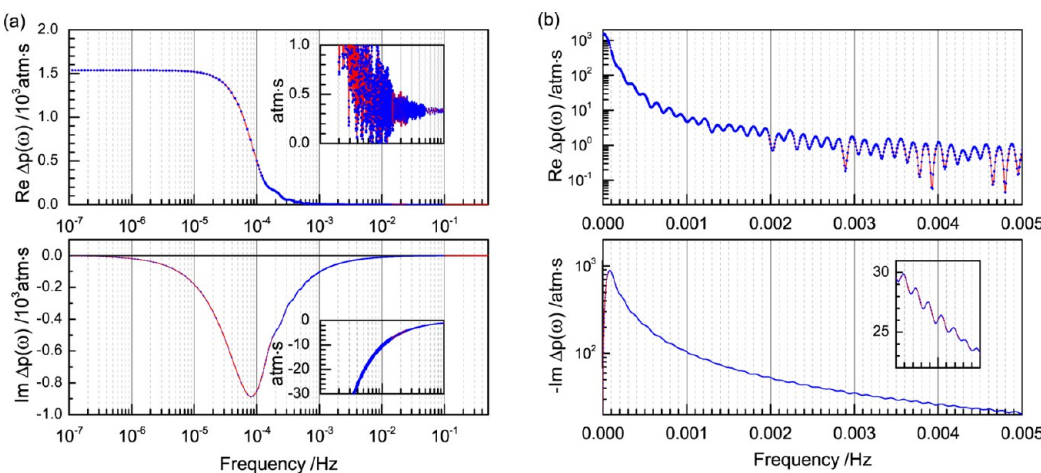


Figure 10. $\text{Re } \Delta p(\omega)$ and $\text{Im } \Delta p(\omega)$ of the Fourier transform of $\Delta p(t)$ of point 17 in linear scale as a function of logarithmic frequencies up to the Nyquist frequency 0.5 Hz (a) and in logarithmic scale as a function of linear frequency up to 5 mHz (b).

Fourier transform algorithms in Origin Pro or Matlab. A macro (which is) programmed in Excel can be convenient for the arbitrary selection of the frequency points in logarithmic scale as well as in

linear scale. The poor quality in raw data as indicated in Figure 9c,d is ascribed to the limited digitized resolution of 0.005 atm of the pressure sensor. The data fluctuate between several pressure

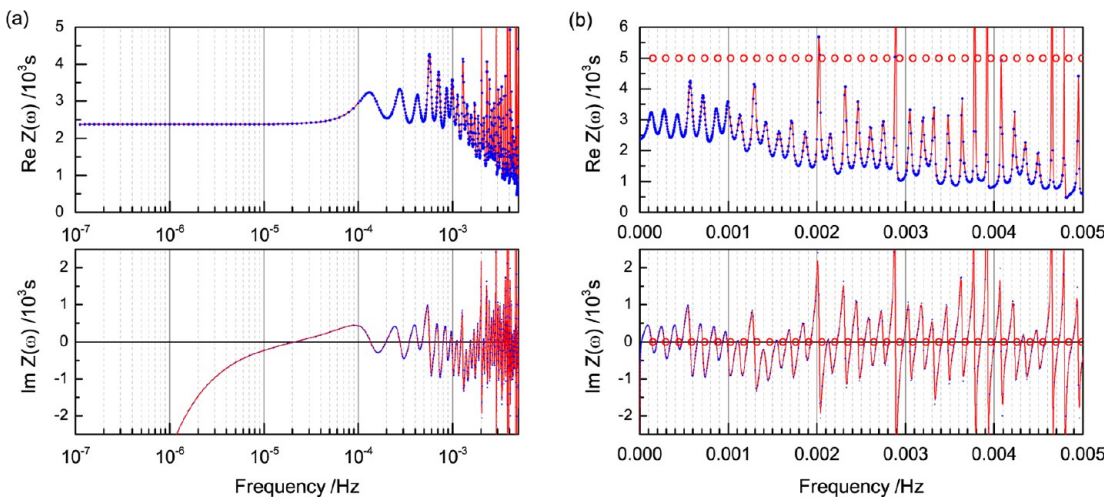


Figure 11. Real and imaginary component of the pneumatochemical impedance Z_{Pn} derived from $\Delta p(\omega)$ in Figure 10 according to eq 18.

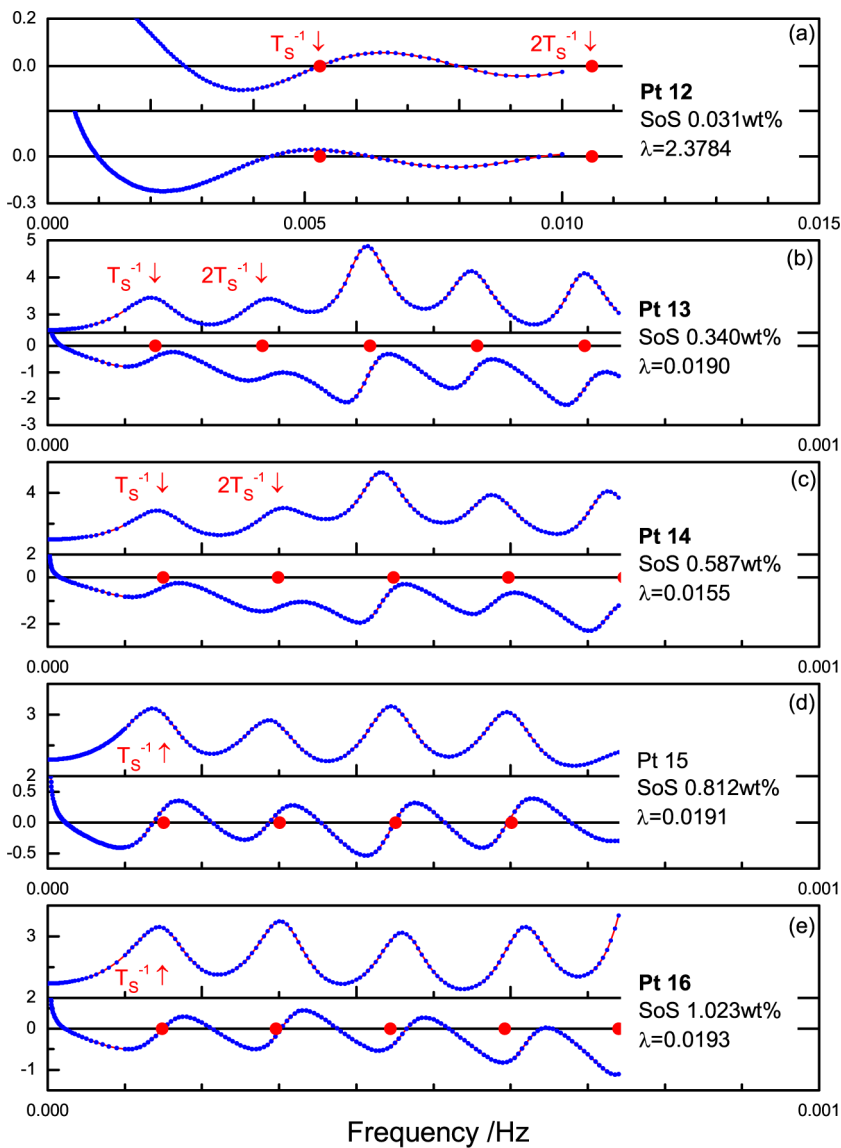


Figure 12. Z' (top) and Z'' (bottom) response as a function of the linear frequencies for the relaxation curves of point 12 in Mg solid solution region (a) and points 13, 14, 15, and 16 (b,c,d,e) in the plateau region up to 1.023 wt % hydrogen.

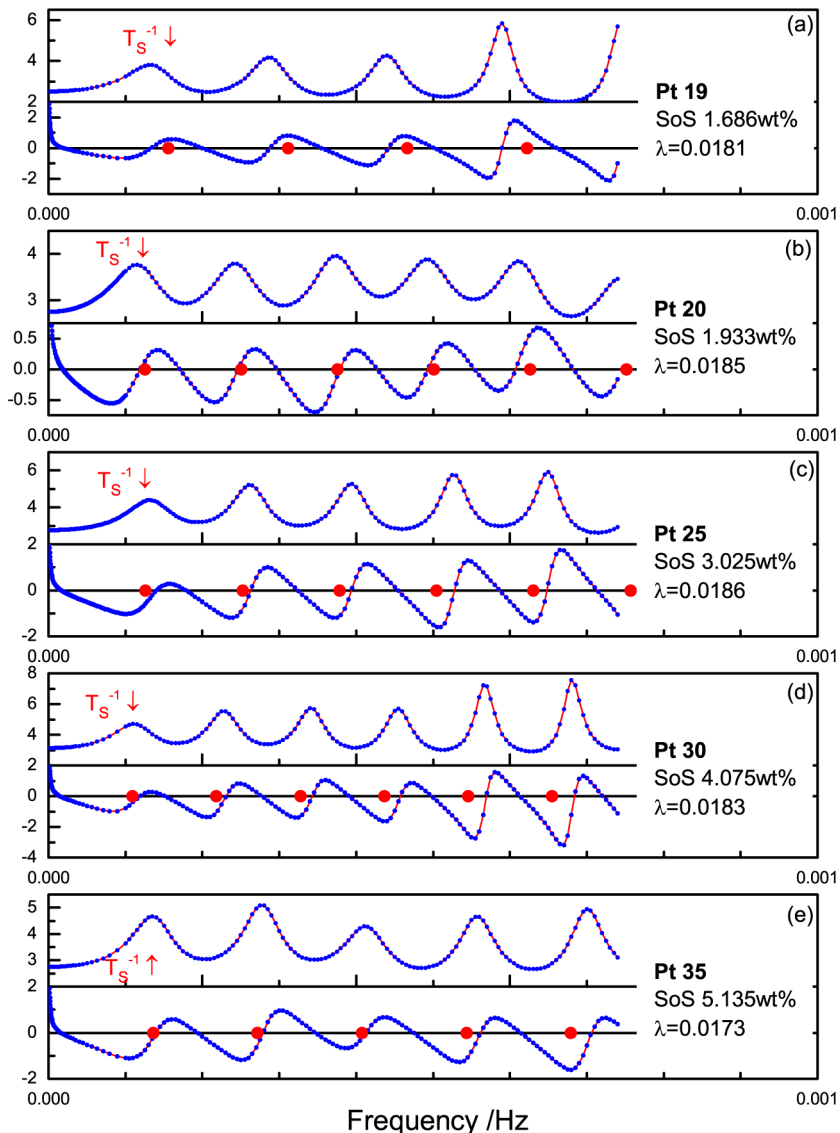


Figure 13. Z' (top) and Z'' (bottom) response as a function of the linear frequencies for the relaxation curves of points 19, 20, 25, 30, and 35 in the plateau region up to 5.135 wt % hydrogen.

steps making constant pressure plateaux over ca. 200 s. The plateau width decreases with the increased pressure variation rate. This is also generally true of any digitized sensing signals. All the relaxation data exhibit similar phenomena when examined closely, but the data in solid solution region with small Δp , suffer most since Δp is very small and the relaxations are comparatively slow. The data smoothing does not affect the evaluation for the frequency range presented below. This is because the integration procedure itself has the effect of data smoothing.

Figure 10 displays an example of $\Delta p(\omega)$ (point 17 as in Figure 9a) in linear scale as a function of the logarithmic frequency (a) and in the logarithmic scale as a function of the linear frequency (b). A Debye-like response as approximately indicated in Figure 10a is consistent with the relaxation curve well-approximated by an exponential decay $\propto \exp(-t/\tau_c)$. The peak frequency of the imaginary component corresponds to τ_c^{-1} . The spectral range is shown up to the Nyquist frequency, $1/2\Delta t = 0.5$ Hz. The spectra continue for the next 0.5 Hz periods symmetrically for the real component and asymmetrically for the imaginary component. The results show that the sampling frequency $\Delta t = 1$ s is high enough to avoid aliasing.^{5,38}

Another notable effect is the persistent oscillation of a constant period of Δf ca. 0.147 mHz as clearly represented in Figure 10b. It is known as Gibbs phenomenon accompanying Fourier transformation of the truncated decay. As well-known for the Fourier transform of the sinc function, $\text{sinc}(f) = \sin(\pi f)/\pi f$ for the time-limited boxcar function, the oscillation reflects the effective time width in the relaxation. The phenomena were also demonstrated for the exponential decay function,³⁸ as in the present data, and the oscillation frequency period, indicated by the circles in Figure 11b, roughly corresponds to the inverse of the sampling time, $\Delta f = T_S^{-1}$, where $T_S = 6820$ s as indicated in Figure 1.

Figures 12–16 show the oscillation behavior of impedance Z' and Z'' for further points of PCI shown in Figure 1. The inverses of the sampling time, T_S^{-1} , shown in Figure 17, roughly correspond to the oscillation frequencies, Δf , indicated in the respective spectra. Note that the sampling time has been automatically determined when the variation in the average pressure of 100 s become less than 0.00025 atm, and thus closely related to the relaxation rate. Figure 17 shows that T_S and τ_c , exponential decay constant coincide with each other almost exactly at point 47. This can be seen in the raw relaxation curve

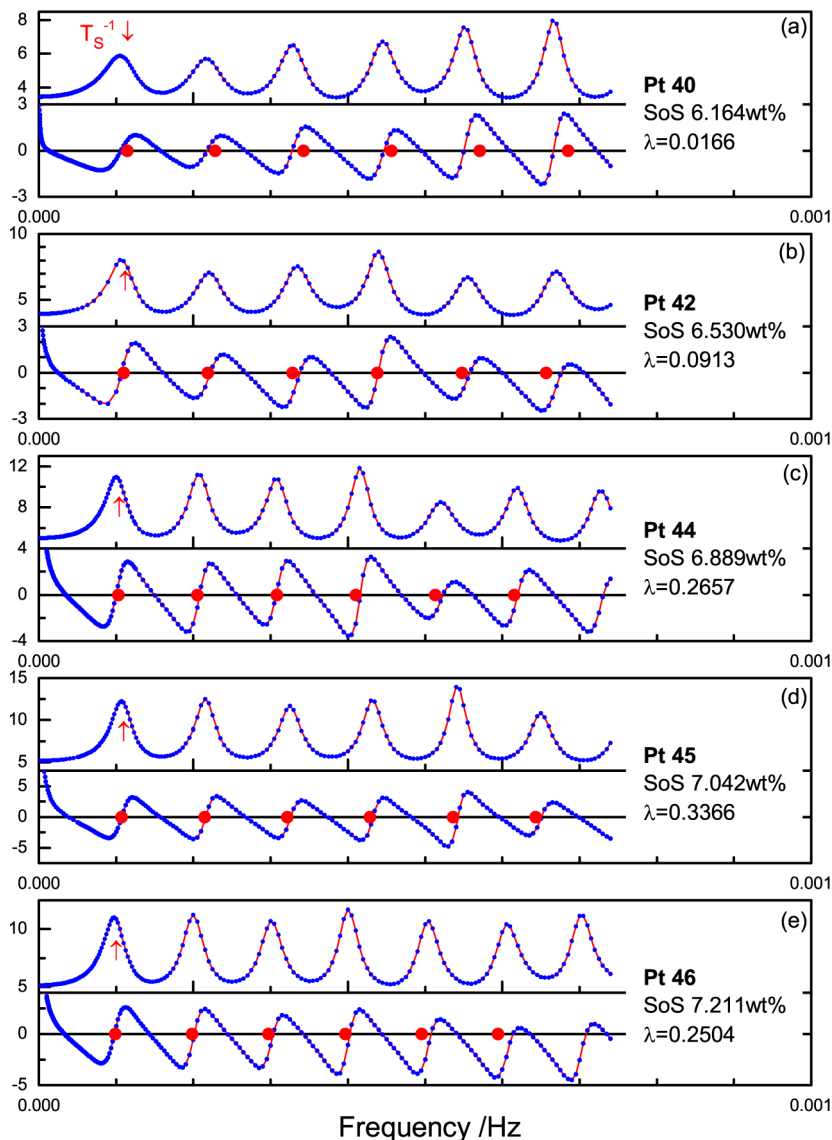


Figure 14. Z' (top) and Z'' (bottom) response as a function of the linear frequencies for the relaxation curves of points 40, 42, and 44–46 for the transition from the plateau to MgH_2 solid solution region.

for point 47 in Figure 1. For the most part of the plateau, e.g., point 17, τ_C becomes shorter than T_S , as also can be noted in the raw relaxation data. For the high pressure region, e.g., point 50, the sampling took place over time less than the exponential decay time. There are irregularities in the oscillation and apparent deviations from the oscillation period determined by the sampling period. Typical irregular features are off-the-beat and out-of-the phase by $1/4\Delta f$ or $1/2\Delta f$. They are prominent for the data of high SoS, from point 49 to 55 as well as point 12 in the Mg solid solution region. It is partly described to the poor quality of the relaxation data due to the limited digitization resolution. The broad band analysis for point 17 also indicates such irregularities at high frequency range, which become reduced when the relaxation data are smoothed by averaging adjacent data. However, the apparent doubling of the oscillation frequency indicated for point 50 in Figure 15 is similar to the simulation with a large resistance value of R rail in the transmission line in Figure 7. The off-the-beat behavior is also described by the c_p element parallel to r , which simulates the attenuation of Z' with increasing frequencies as in the experimental data.

Therefore, it can be concluded that the experimental pneumatochemical impedance exhibits the features of RL two-rail transmission line model. Although the oscillation originates from the arbitrary sampling periods, the kinetic information intrinsic for the sample and the experimental condition is expected to be deconvoluted from the impedance behavior. Possible remedies to avoid or reduce the artifactual oscillation behavior are monitoring for a sufficiently long time⁵ or adding the long-time relaxation tail in the data treatments.¹⁸ The former may be not be practically nor perfectly applied. The latter, due to the volumetric requirements, cannot be applied for the pressure relaxations.

Pneumatochemical Immittance. As discussed previously (see Figure 5 and eq 8), the force-flow correlation in the hydrogen storage kinetics by the volumetric method leads to the inductive nature in the pneumatochemical impedance formulated according to eq 18. Figure 11 shows how the capacitive Z'' evolves into the inductive Z'' from $\Delta p(\omega)$ shown in Figure 10. It should be noted that the impedance behavior below 10^{-4} Hz or 0.1 mHz is not ascribed to the oscillation behavior but the

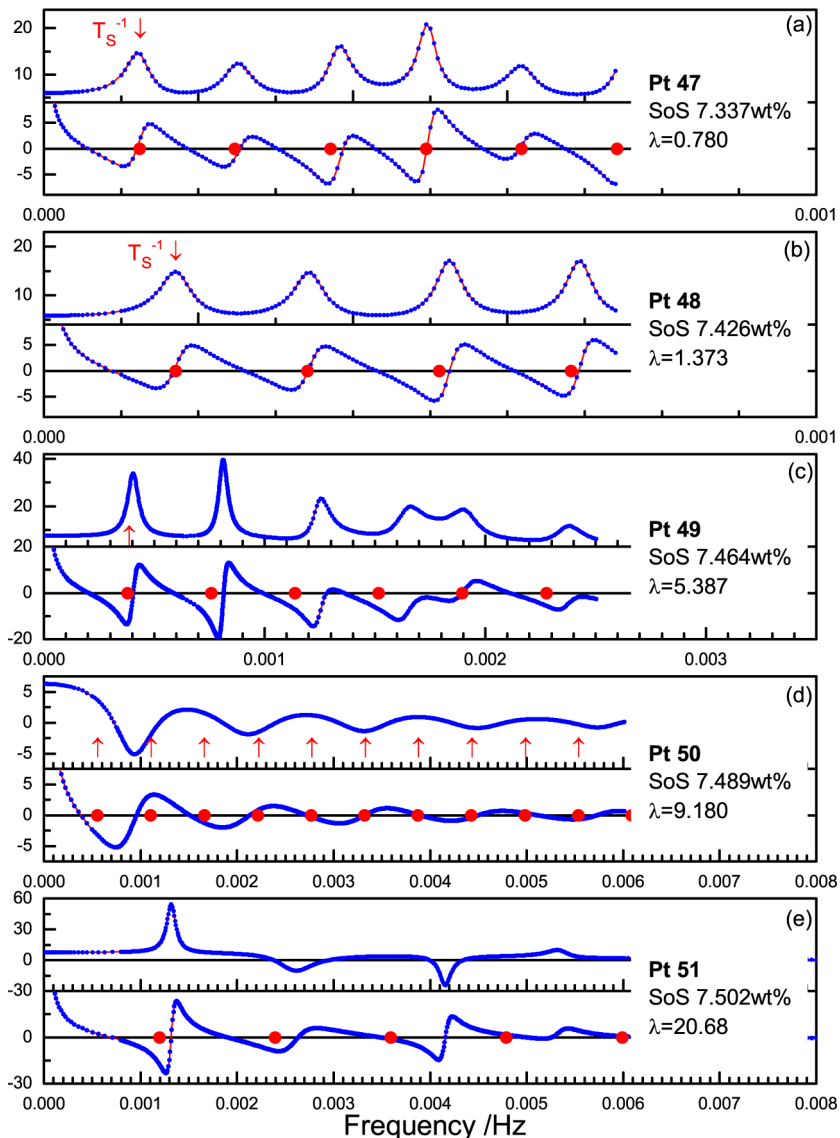


Figure 15. Z' (top) and Z'' (bottom) response as a function of the linear frequencies for the relaxation curves of points 47 to 51 in MgH_2 solid solution high pressure region.

consequence of the formulation of the pneumatochemical impedance. This feature does not appear in PIS by Millet et al.^{3,5} since the separate pressure $p_2(t)$ is monitored in the sample chamber, while $i(t)$ is evaluated from the pressure relaxation $p_1(t)$, which is conventionally singly monitored. The two pressure values are, however, correlated by the mass flow controllers between chambers and the high frequency response in the pneumatochemical impedance, apparently looking like the ohmic and charge transfer impedance in Figure 3, originates from the experimental setup for the two pressure measurements, not related with the hydrogen storage kinetics of the material system.

In Figure 11, Z'' is shown to change from capacitive to inductive between 10^{-5} and 10^{-4} Hz, and then again to capacitive and so on in the oscillation period of ca. 0.15 mHz, with out-of-phase simultaneous variation of Z' circular impedance trajectories result as shown in Figure 18a. Up to the frequency 1 mHz, approximately six circular loops are present as indicated by the Roman numerals near Z''_{\max} . Different representations of the same spectrum are presented in Figure 18. As well as capacitance plots of $C_{pn} = (j\omega Z_{pn})^{-1}$ (b) employed in the previous section,

admittance $Y_{pn} = Z_{pn}^{-1}$ (c) and modulus $M_{pn} = C_{pn}^{-1}$ (d) are shown in complex plane representation, and immittance is the general term for different representations.^{35,39} Specific aspects of the frequency response are more clearly visualized in one or the other representations. Note that the unit of pneumatochemical impedance is time in seconds in the present definition, according to eq 15, and pneumatochemical capacitance has no unit.

The characteristics of Z_{pn} can be best examined from the low frequency range. At low enough frequency, $\omega \rightarrow 0$, Z_{pn} becomes

$$Z_{pn}(\omega \rightarrow 0) = \frac{\Delta p(\omega)(\omega \rightarrow 0)}{\Delta p_j} + \frac{(p_j - p_{j-1})}{j\omega \Delta p_j} \quad (19)$$

Note that $(p_j - p_{j-1})$ and Δp_j are the constants determined by the PCI curve. Z'' corresponds to the response of the capacitance $C_S = \Delta p_j/(p_j - p_{j-1})$. The capacitance is the inverse of λ parameter. They are given from PCI, as shown in the inset of Figure 1 and put as constants in the evaluation of the pneumatochemical impedance Z_{pn} . From the RC transmission line model for diffusion, C_S corresponds to the chemical capacitance C_d

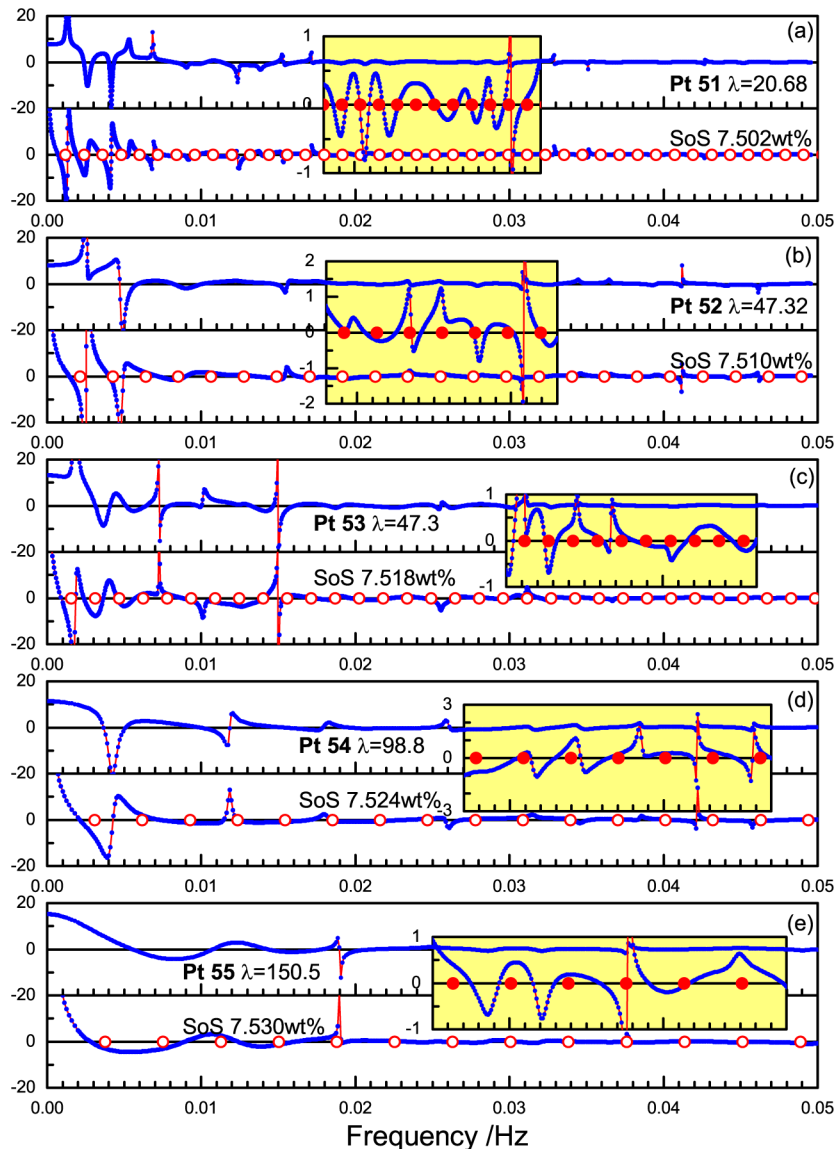


Figure 16. Z' (top) and Z'' (bottom) response as a function of the linear frequencies for the relaxation curves of points 51–55 in MgH_2 solid solution high pressure region. For point 51, the frequency range is increased to 50 mHz from 6 mHz in Figure 15e.

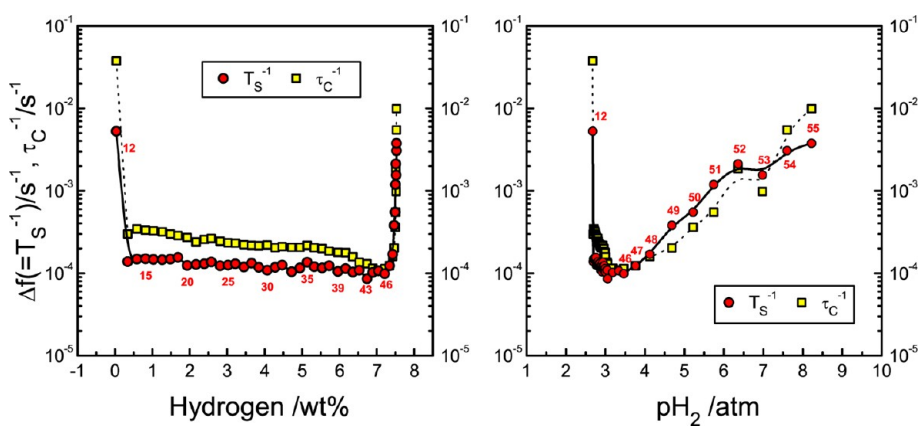


Figure 17. Oscillation intervals Δf compared with the exponential decay constant τ_C of the raw data in Figure 3.

(see Figure 3), which corresponds to the thermodynamic contribution in chemical diffusivity, $\tilde{D} = a^2/(3R_dC_d)$, eq 7. Since $\Delta p(\omega)$ is purely real, constant for the low frequency range as shown in

Figure 10, Z' becomes also constant series resistance, $R_S = \Delta p(\omega)/\Delta p_j$. This is shown in the inset of Figure 18a by the line response parallel to Z'' -axis. Therefore, the impedance behaves as

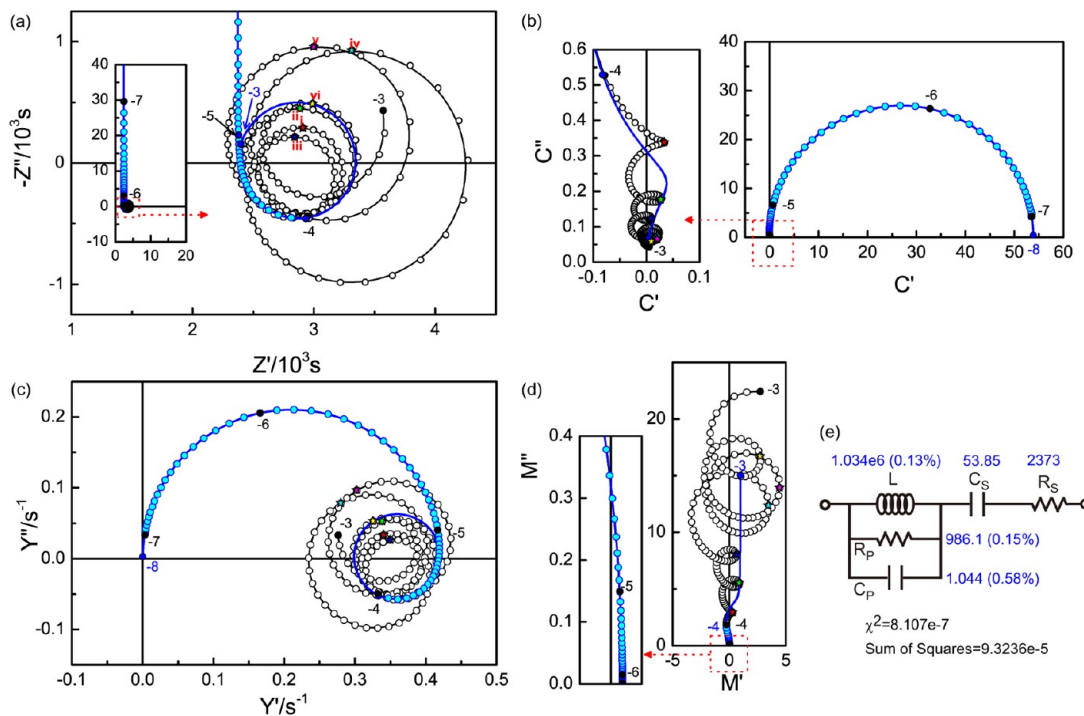


Figure 18. Pneumatochemical immittance spectra for the relaxation curve of point 17. (a) Complex impedance plane presentation ($Z' - Z''$) of the high frequency spectrum for $f \leq 1$ mHz with the full spectrum from 10^{-7} Hz as an inset. (b) Complex capacitance spectrum ($C' - C''$) where the inset presents the high frequency details near the origin. (c) Corresponding admittance spectrum ($Y' - Y''$). (d) Modulus spectrum ($M' - M''$) with the magnified low frequency region near origin. (e) Equivalent circuit model and fit results using the data range ≤ 0.1 mHz (data points filled in cyan color). The simulation using fit results for $f \leq 10$ mHz is indicated in blue lines. The numbers for the filled symbols are logarithmic frequencies.

the series circuit of $C_S - R_S$, which can be seen as part of the equivalent circuit model in Figure 18e.

The semicircular trace of the simulation of RL two-rail transmission line model for one-dimensional diffusion in Figure 6e was shown to provide the approximately correct R and L input parameter by fitting using LR parallel circuit of lumped elements, if R and C values are sufficiently large. The R parameter is the pure kinetic parameter in the chemical diffusivity, $\tilde{D} = a^2 / (R_d C_d)$. It should be examined whether and how R parameter for the kinetic contribution in chemical diffusivity can be obtained from the experimental pneumatochemical impedance of an Mg/MgH₂ system. To check the possibility of the model-based analysis, the Kramers–Kronig compliancy was tested numerically using the test program (kktest.exe) provided by Boukamp.^{40,41} Figure 19 shows that when the frequency range is limited below 10^{-4} Hz, the residuals become essentially zero. Note that the poor KK compliancy above 10^{-4} Hz does not necessarily exclude the model analysis for the high frequency oscillating response. The oscillatory response of the RL two-rail transmission line model for one-dimensional diffusion can be also fitted. The present numerical KK algorithm is not capable of handling the oscillatory response since it is based on the nonlinear least-squares fitting with conventional KK-compliant elements such as R , C , L , and constant-phase-element (CPE) Q with $Z_Q^* = [A(i\omega)^\alpha]^{-1}$. This is also the reason for the strong dependence on the frequency range shown in Figure 19.

Although the simulation using RL two rail transmission line model successfully addresses the important aspects of the pneumatochemical impedance, for the analysis of the experimental results more developments are necessary. Equations 6 and 7 show that the formulation become rather involved for the spherical diffusion even for the diffusion impedance. Therefore,

in the present work an equivalent circuit consisting of the lumped elements only is employed for the frequency range up to 10^{-4} Hz.

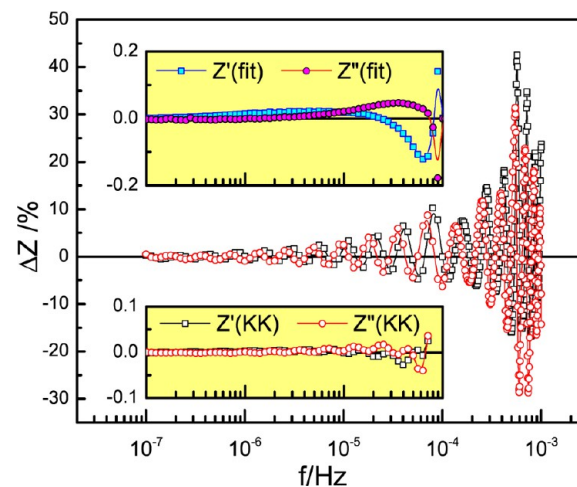


Figure 19. Kramers–Kronig test residuals for the pneumatochemical impedance for point 17 for the frequency range from 10^{-7} to 10^{-3} Hz and for the upper limit of 10^{-4} Hz in the inset at the bottom. Inset at the top presents the errors from the fitting using the equivalent circuit model presented in Figure 18.

An equivalent circuit of ideal lumped elements of L , C , and two R elements, i.e., $R_S C_S$ series circuit for the low frequency limit and with $R_P C_P$ parallel circuit for the high frequency inductive loop in series, is shown to describe the spectrum with KK residuals less than 1%. Additional parallel capacitance C_P reduces the residuals even less than 0.1% as shown by the inset at the top of Figure 19. The addition of the parallel capacitor C_P is in line with the

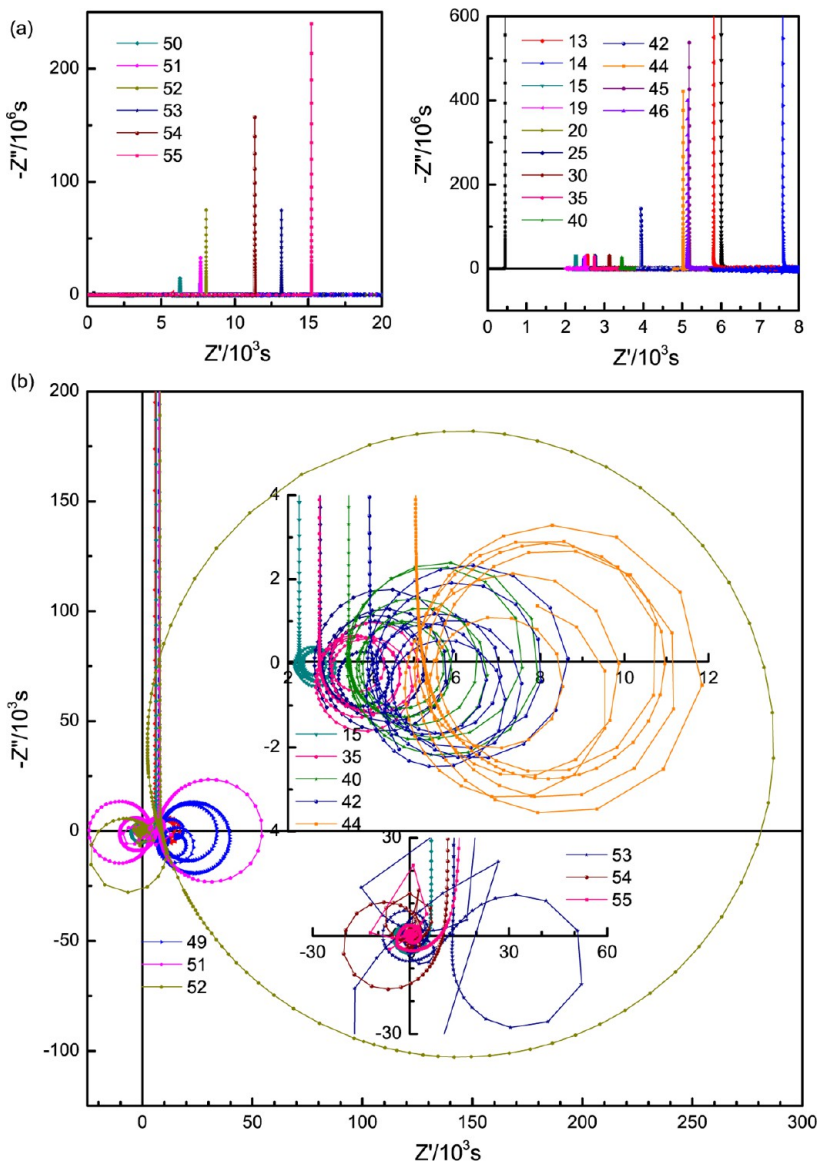


Figure 20. Selected pneumatochemical impedance spectra. The graphs in panel a represent the capacitance dominated impedance spectra evaluated down to 10^{-7} Hz where the spectra with smaller capacitance and with larger capacitance are distinguished in the left and right graphs, respectively. Note that the spectra are not drawn isotropic. High frequency region near Z' -axis is shown in panel b. The main graph and the inset at lower part indicate the behavior of MgH_2 solid solution region. The top inset represents the behavior of the plateau region.

modified transmission line model in Figure 4d, which was included to describe the Z' attenuation at high frequencies. It should be noted that all components are basic lumped circuit elements of L , R , and C . No Q element with $\alpha < 1$ is applied.

Figures 20 and 21 present Z_{pn} and C_{pn} in complex plane derived from the point relaxations in Figure 1. The frequency dependence of Z' and Z'' are also presented in Figures 12–16. The fit results using the equivalent circuit demonstrated for the point 17 are presented as a function of SoS in Figures 22 and 23. The left and right columns represent the dependence on the hydrogen SoS and pressure, respectively. The fitted C_s , which corresponds to C_d of the RC transmission line model for diffusion, is shown to be consistent with λ^{-1} , which is pre-determined from PCI and used in the evaluation of pneumatochemical impedance according to eq 18. The variation of C_s is compared with τ_{pn} obtained by the time-domain analysis⁹ to indicate the thermodynamic contribution by C_d since $\tau_{\text{pn}} = a^2 / \tilde{D}$ and $\tilde{D} = a^2 / (3R_d C_d)$. The variation of τ_{pn} and \tilde{D} with respect to

C_p should be explained by R_d . Comparison of the magnitude of \tilde{D} from τ_{pn} confirms the equality $R_d = R_p$ same as the simulation with RL two-rail transmission line model for one-dimensional diffusion. The equality is also illustrated by evaluating the equivalent $R_d(\text{PnITT})$ from \tilde{D} and τ_{pn} . Note that $R_d(\text{PnITT})$ is shown by the axis scale shifted for clarity. The parameter $R_p (= R_d)$ then represents the hydrogen self-diffusivity, D_H , the kinetic contribution in \tilde{D} , since $D_H = \tilde{D} / \lambda = \tilde{D} C_d = a^2 / (3R_d)$. The D_H (R_p) is shown to decrease (increase) in the plateau region of the two-phase coexistence and further decrease in the MgH_2 solid solution region. As previously discussed for the equivalent results from the time domain analysis,⁹ the variation of the diffusivity in the plateau region can be explained by the hydride phase formation controlled by slow diffusion through the hydride according to shrinking-core model.⁴² For the parameter R_p alone, one may not need to perform the parametric analysis at all. The impedance spectra in Figure 20 indicate the circular traces, and R_p can be graphically read out without much loss in the accuracy

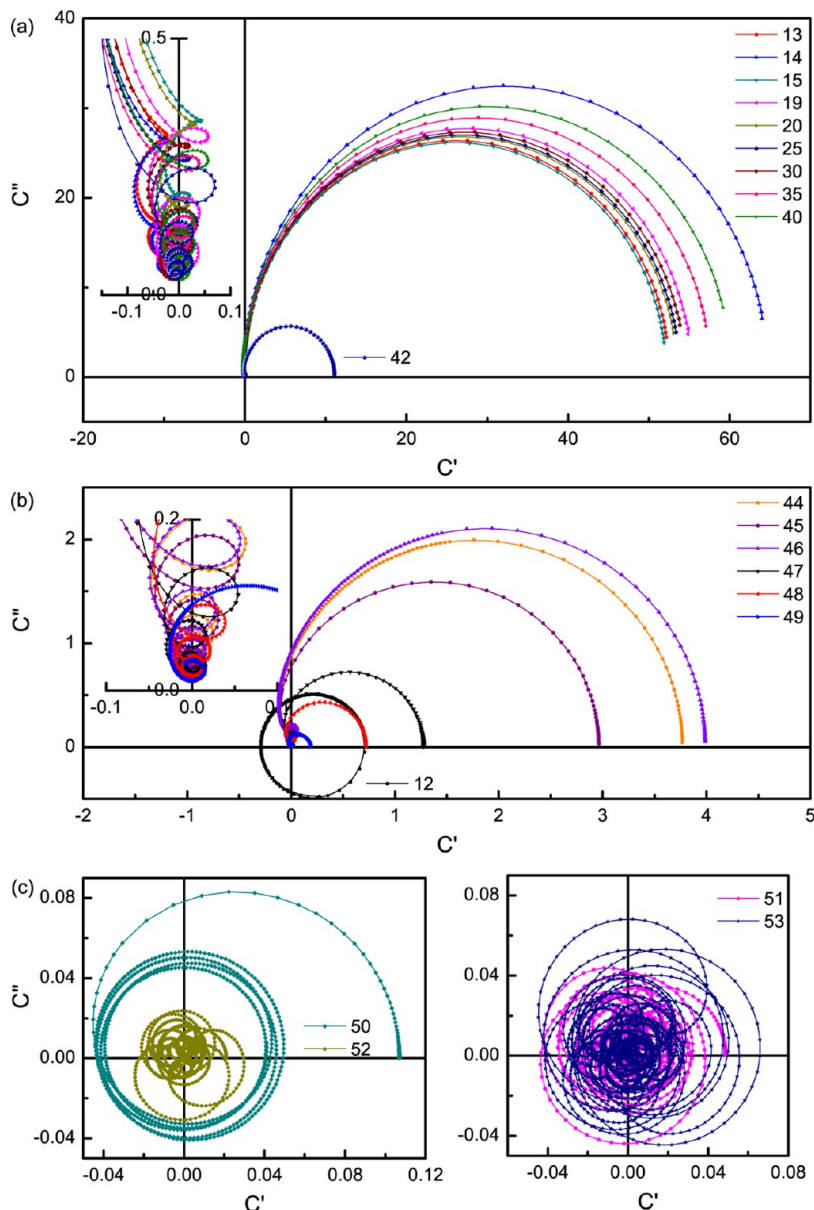


Figure 21. Selected pneumatochemical capacitance spectra. The spectra in panel a represent those with large capacitance values. Inset indicates oscillations at high frequency. The spectra in b and c show the cases with smaller capacitance values, where the high frequency inductive behavior and oscillation become more visible and even dominating.

since the fitting analysis has also limitation in the frequency range. The impedance spectra clearly indicate the increase in size for the points in the plateau region as points 15, 35, 40, 42, and 44. The graphical read-out resistance R_p and \tilde{D} therefrom are presented in Figure 23. The increase in R_p in the high pressure MgH₂ solid solution region is also clearly visualized. The formation of inductive loops in the opposite direction should be noted. They are also indicated in the frequency dependence of Z' , which resonates either in the opposite direction or off the beat, e.g., point 12 in Mg solid solution region in Figure 12 and points 50–55 in MgH₂ solid solution region in Figures 15 and 16. For fitting, negative R values are used, and the absolute magnitude or the amplitude is considered to represent the equivalent kinetic effects as shown by the shaded data points of R_p and therefrom derived \tilde{D} .

The parameter R_p is thus the single parameter derived by the parametric analysis for the chemical diffusivity and hydrogen

diffusivity since C_S is essentially predetermined by λ values from PCI. Similarly, although other parameters such as Δp_i and p_j were also fitted together, τ_{pn} was the only parameter of interest for the kinetic information from the time-domain analysis. In the case of parametric analysis of the pneumatochemical impedance, due to the novelty of the method, it should be interesting to examine the characteristics of other parameters such as L , R_S , and C_P , which are presented in Figures 22 and 23. The most interesting parameter of the present analysis should be the inductor L . In the LC transmission line model for one-dimensional diffusion, the oscillation period is $(2(LC)^{1/2})^{-1}$, and the oscillation behavior is shown to be affected by R_d and additional C_P (Figures 7 and 8). It was found that the inductor of the simple equivalent circuit employed in the present work represents the variation of τ_C , the exponential decay time, almost exactly as $3\sqrt{L} = \tau_C$ as shown in Figure 22b. The apparent decay constants τ_C were also more or less similar to the lead time Δt in the time domain fitting⁹ as

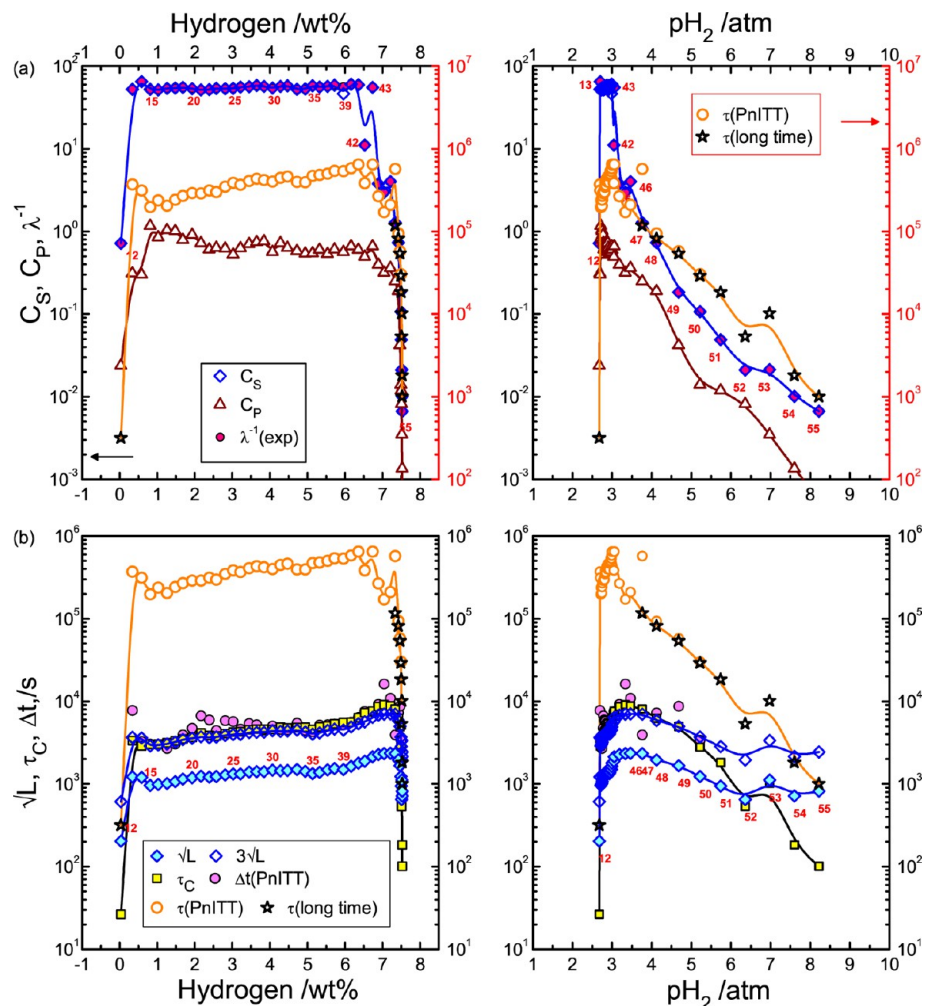


Figure 22. Fit parameters C_p , L . Left graphs represent the dependence on the hydrogen composition or state of storage (SoS) and right graphs on the hydrogen pressure. (a) The capacitance C_s and C_p of the equivalent circuit in Figure 18e where $C_s = \lambda^{-1}$. The τ parameter from the time-domain analysis (PnITT) is also presented for comparison. (b) The inductance values can be related to exponential decay constant τ_c , which are also comparable to the adjustment time Δt in the time domain analysis (PnITT) as $3\sqrt{L} = \tau_c \approx \Delta t$.

shown in Figure 2c,d. Therefore, L parameter is considered to represent the true relaxation of the data, not related to the arbitrary sampling time, T_s . This may be understood from the Fourier transform of $\Delta p(t)$, $\Delta p(\omega)$, and the impedance Z_{Pn} therefrom shown in Figures 10 and 11, where the inductive response is closely related with the Debye-like transition of $\Delta p(\omega)$. As may be expected that the oscillating frequency periods should bear a close relationship with C_p parameter, which is shown to describe the higher frequency response on the verge of the oscillatory response. Indeed, Δf is shown to be almost exactly consistent with $6((LC_p)^{1/2})^{-1}$, Figure 24. The dependence of C_p on SoS should be understood as adjustments for Δf with respect to L contribution. It seems like that the oscillation effects originating from the truncation effects can be thus described by $L-3C_p$ transmission line model, rather than $L-C_s$, where L represents the true relaxation effects and C_p parameter describe the truncation artifacts in the data sampling. The dc limit resistance $R_s = \Delta p(\omega)/\Delta p_j$ was defined in eq 19. The parameter can be evaluated essentially with zero error similarly as C_s . The R_s is shown to be comparable to R_p in Figure 23a. For the ideal RC transmission line model for the spherical diffusion, the R_s in series with C_p should be $1/5R_d$ or $1/5R_p$ as shown in Figure 3. In the high pressure region displayed in Figure 23b, R_s

is shown indeed correspondingly lower than R_p . However, in the plateau region R_s is shown larger than R_p especially in the low hydrogen region. This may be ascribed to the additional impedance at the high frequency region, e.g., by nucleation and interface/surface reaction, which is consistent with the higher R_s in the lower hydrogen region where the hydride phase nucleates and starts to grow. Parametric analysis provides more information on the hydration kinetics. The diffusion limited kinetics can be more reliably obtained from R_p parameter rather than R_s parameter.

Automated Hydrogen Storage Kinetic Analysis. Time-domain analysis based on the error function solution (eq 3) suffers from the heavy calculation of the error functions, which is also numerically limited for large numbers.⁹ The substantial lead-time necessary for the modeled diffusion process makes the analysis very sensitive to the initial values. The outlier as point 47 and the large error of point 49 in the right graph of Figure 23b indicates such difficulty. For the poor digitization quality data in high pressure region, even the simple exponential fitting for the long time solution can be performed only with proper initial values and bounds for the fitted parameters. The τ parameters obtained thereby, except obvious outliers, are shown physically significant.

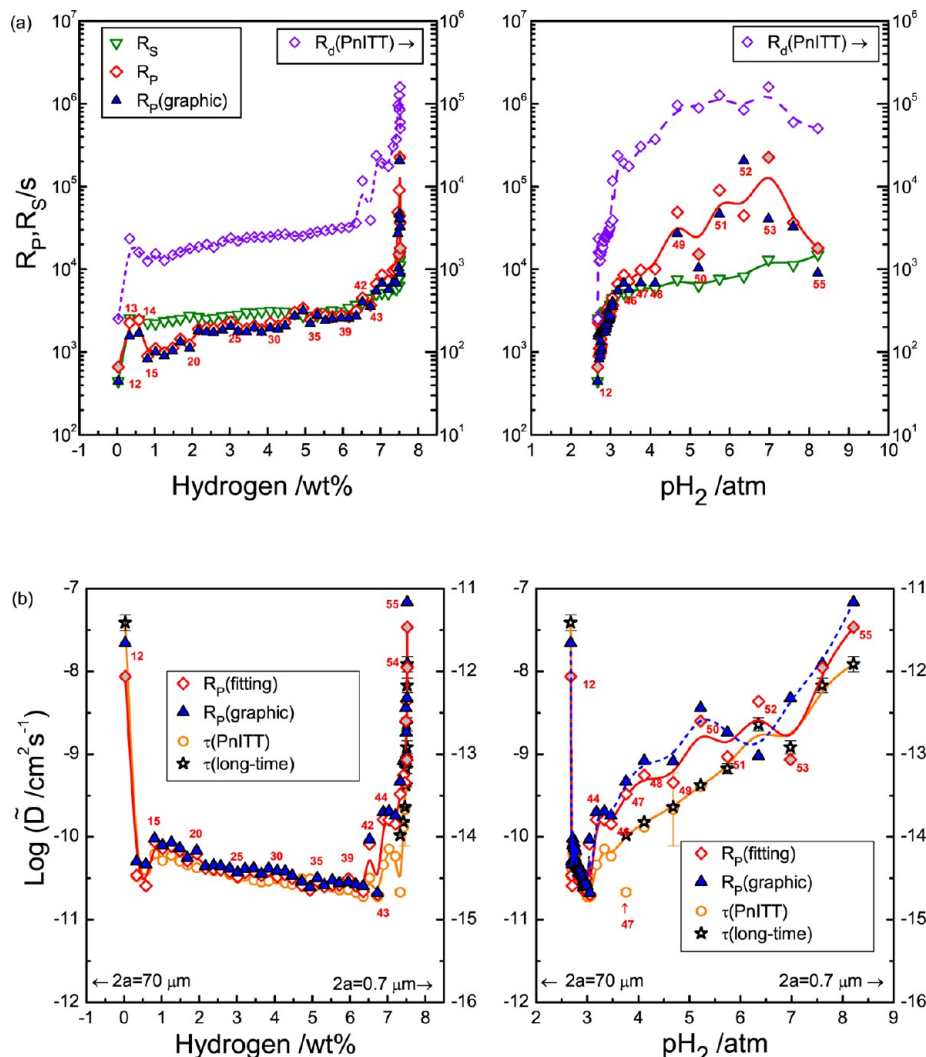


Figure 23. (a) Resistance elements R_S vs R_P from PnIS compared with equivalent R_d from PnITT. (b) Chemical diffusivity values from $\tau = 3R_P C_S$ for $a = 70 \mu\text{m}$ (left axis) and $0.7 \mu\text{m}$ (right axis) compared with the results from the time-domain analysis. For clarity, $R_d(\text{PnITT})$ is shifted by 1 order of magnitude. Left graph represents the dependence on SoS and right on the pressure.

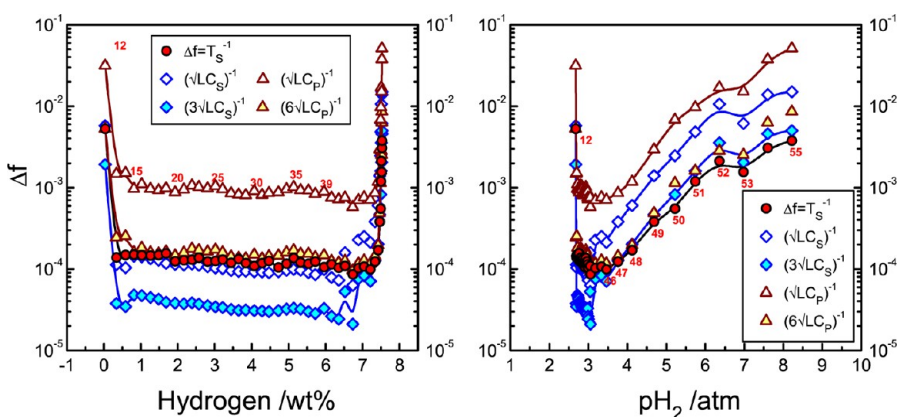


Figure 24. Oscillation intervals Δf compared with $((LC_S)^{1/2})^{-1}$ and $((LC_P)^{1/2})^{-1}$. Left graph represents the dependence on SoS and right on the pressure.

However, the pneumatochemical impedance according to Figure 18 can be reproducibly obtained for an arbitrary frequency value without paying attention to the quality of the raw data. All the spectra also exhibit a smoothly varying frequency response as shown in Figures 12–16 and in the complex plane plots of

Figures 20 and 21, when the frequency points are appropriately chosen for the oscillating frequency regime. Model analysis with a very simple equivalent circuit was also quite successful as the parameters can be well-correlated with those much more painstakingly obtained by the time-domain analysis. For the

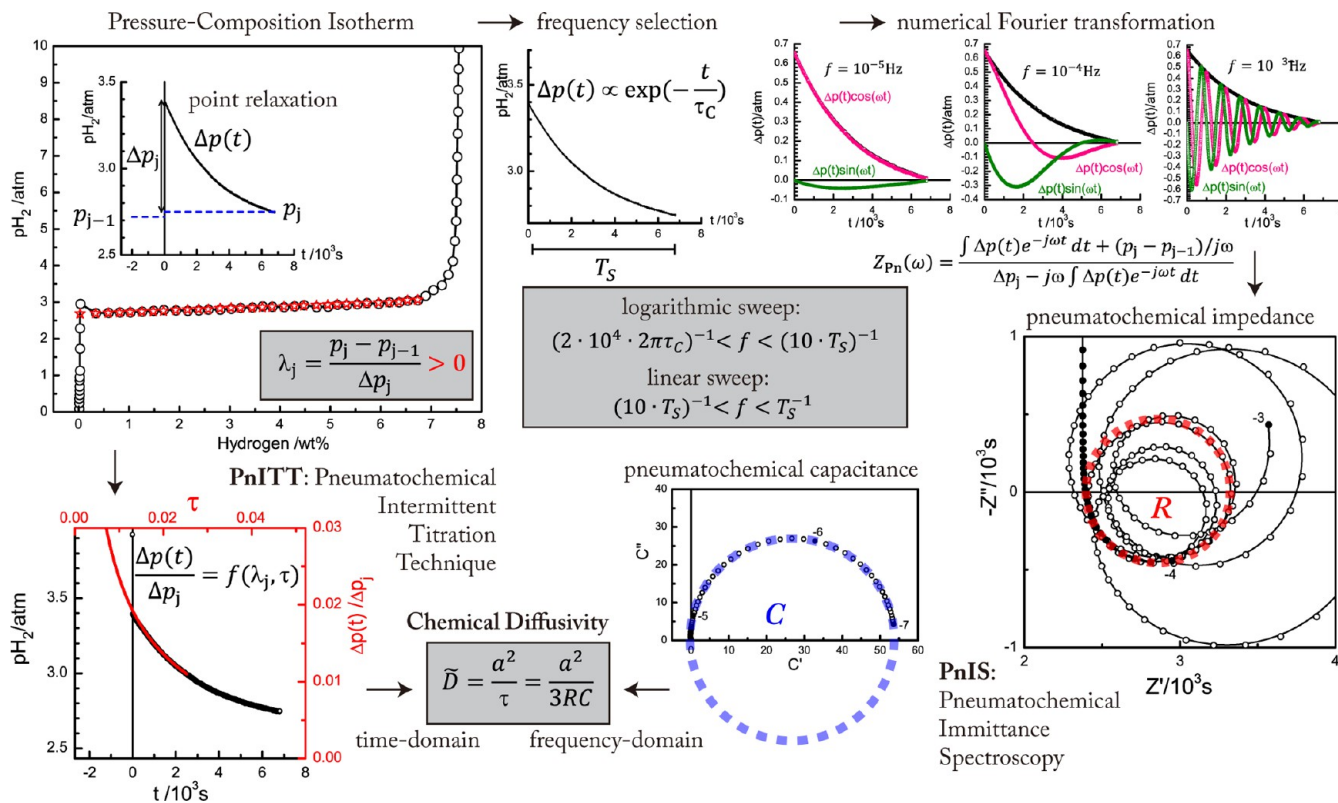


Figure 25. PCI from p_j , corrected for $\lambda > 0$, and Δp_j and point relaxations $\Delta p(t)$ raw data (top left). Frequency selection for logarithmic and linear sweep based on the decay constants and the sampling periods (top middle). Numerical Fourier transformation of the relaxation curve and Z_{Pn} evaluation (top right). R , from the inductive loop of the pneumatochemical impedance, PnIS (bottom right), and $C = \lambda^{-1}$, the size of the capacitance arc, give chemical diffusivity $\tilde{D} = a^2/3RC$ (bottom middle) which is consistent with $\tau(\tilde{D})$ from diffusion solution $\Delta p(t) = f(\lambda, \tau)$ by time domain analysis, PnITT⁹ (bottom left).

estimation of R_p parameter only, which gives the information equivalent to τ_{Pn} parameter by time-domain analysis, even the circuit fitting may not be necessary since R_p is clearly visualized by the inductive loops in the impedance plane.

The diagrams in Figure 25 illustrate the essence of the pneumatochemical kinetic analysis developed in this work, which can be almost fully automated up to the systematic procurement of the chemical diffusivity as a function of SoS. Top left shows the pressure composition isotherm obtained by measurements of point relaxations in a conventional Sievert's setup. This procedure has been automated in most PCT setups. The isotherm is constructed by the equilibrium pressure p_j and the pressure drop Δp_j for the hydrogen absorption amount from each point relaxation curve.

For the kinetic analysis both in the time domain⁹ and in the frequency domain, $\lambda_j = (p_j - p_{j-1})/\Delta p_j$ is the key parameter. This value should be positive. However, the plateau region generally with very small variation in p_j the value may fluctuate. Since the plateau region experimentally measured exhibits nonzero positive dependence on average, a linear regression may be used for $\lambda_j > 0$. Since the variation in p_j is very small compared to Δp_j in the plateau region, hydrogen absorption estimates from Δp_j may remain unaffected. In fact, the finite λ values in the plateau region may represent the kinetic features but depend on the sampling times and cutoff criteria and thus are not well-defined in view of thermodynamics. The diffusion formalism based on the λ values is nonetheless valid and the kinetic parameters derived were shown to be physically significant.⁹

With given λ values, τ_{Pn} can be evaluated by fitting $\Delta p(t)$ to the error function solution, eq 3, or other approximate solutions depending on λ values for the diffusion problem of a solute in a limited amount under constant volume condition (bottom left). It is named as PnITT, pneumatochemical intermittent titration technique, since it allows the determination of the chemical diffusivity from the intermittent hydrogen injection similarly as intermittent titration techniques in the electrochemical storage kinetics.⁹

The frequency-domain response by Fourier transformation of $\Delta p(t)$ can provide equivalent kinetic information. Millet et al.^{1–5} suggested PIS, pneumatochemical impedance spectroscopy employing a special two-pressure monitoring setup. Analysis based on the single pressure signal developed in the present work is named as PnIS, pneumatochemical immittance spectroscopy. The pneumatochemical impedance exhibits the inductive response by definition according to eq 18 displayed, and the further oscillation is due to the truncation in sampling the relaxation. The size of the inductive loops and first circular traces provides R parameter for the chemical diffusivity, $\tilde{D} = a^2/(3RC)$. The λ parameter predetermines C as λ^{-1} , which may be also visualized by the capacitance spectrum.

The key step for the full automation of the kinetic analysis up to the visualization or even the automatic graphical estimation of R parameter is to select appropriate frequency range for the well-behaved spectra. For the capacitance plots and also possible parametric analysis, the frequency range should be taken logarithmically over decades. For the Debye response of $\xi(\Delta p(t))$ of the exponentially decaying $\Delta p(t)$ with time constant τ_C , as shown in

Figure 10, down to 0.1% of $\text{Im } p(\omega)$ can be obtained at frequency ca. $(2 \times 10^4 2\pi\tau_C)^{-1}$. For the point 17 with $\tau_C = 3140$ s, the lower boundary of the frequency can be set at ca. 2.5×10^{-8} Hz. As shown in the capacitance spectrum at the bottom (see also Figure 18b), the frequency value is sufficiently low to visualize the circular capacitance spectrum for the C parameter. (In the case of small C parameters where the high frequency response dominates as in Figure 21c,d, dc limit value of C should be taken.) The high frequency limit for the logarithmic frequencies can be set as ca. $(10 \cdot T_S)^{-1}$, i.e., one order lower than the oscillating period, $\Delta f = T_s^{-1}$, since the oscillatory behavior can be shown by the linear frequency intervals. Since $T_S = 6820$ s and thus $\Delta f = 1.5 \times 10^{-4}$ Hz, the frequency values may be chosen from ca. 1.5×10^{-5} Hz with the interval, e.g., $\Delta f/10$, to produce the smooth circular trace as shown in the bottom right (see also Figure 18a). For the evaluation and visualization of the R parameter, calculation up to T_s^{-1} is usually sufficient. Note that the big circular response of point 50 in Figure 20 of almost hundred frequency points is evaluated for the smooth trace. For many oscillatory traces presented in Figure 11 or Figures 12–16, the number of frequency points becomes very large as hundreds or thousands, and the fast Fourier transform algorithm can be employed.

CONCLUSIONS

A frequency-domain analysis has been successfully performed as a sequel to our recent report on the time-domain analysis for the determination of the chemical diffusivity from the pressure relaxations monitored in a conventional Sievert's setup. The formulation of the pneumatochemical impedance with a force-flux correlation as the hydrogen flux being proportional to the pressure variation by the constant volume condition leads to a characteristic inductive loop behavior, where the L parameter indicates the exponential relaxation as $3\sqrt{L} \approx \tau_C$ and the R_p parameter of the RC transmission line model for diffusion, which determines the chemical diffusion coefficient for the spherical diffusion as $\tilde{D} = a^2/(3R_pC_S)$ where the low frequency limiting C_S parameter is predetermined by the pressure-composition isotherm. The evaluation is shown consistent with the chemical diffusivity determined by τ_{p_n} from the time-domain analysis as $\tilde{D} = a^2/\tau_{p_n}$. The inductive loops further develop into circular oscillatory traces, which can be ascribed to the truncation effects in the sampling of the relaxation curve. The RL two-rail transmission line model simulates essential characteristics of the experimental pneumatochemical impedance: R parameter indicated by the inductive loop and the generation and the modulation of the oscillation behaviors.

While the error function fitting in the time-domain analysis is rather calculation-intensive and sensitive to the initial values, the frequency domain analysis can be almost automatically performed up to the visualization of the R and C parameters for the chemical diffusivity with the suggested proper criteria for the selection of the frequency points in logarithmic and linear intervals. A simple equivalent circuit modeling employing only ideal lumped elements for the first inductive loops provides information more than R_p parameter. The series resistor R_S parameter was shown to correspond to theoretical $1/5R_p$ in the solid solution region but indicate the nucleation and/or interface reaction in the two-phase region. The C_p in parallel to $L-R_p$ improves the high frequency description and represents the sampling period $T_S \approx 6(LC_p)^{1/2}$.

AUTHOR INFORMATION

Corresponding Author

*(J.-S.L.) E-mail: jongsook@jnu.ac.kr. Phone: +82 (0)62 5301701. Fax: +82 (0)62 5301699.

Notes

The authors declare no competing financial interest.

ACKNOWLEDGMENTS

This work was supported by the Basic Research Laboratories (BRL) Program (No. 2009-0085441) of the National Research Foundation of Korea (NRF) funded by the Ministry of Science, ICT & Future Planning.

REFERENCES

- (1) Millet, P.; Dantzer, P. A New Approach to the Kinetics of $\text{LaNi}_5-\text{H}_2(g)$ Systems Based on Impedance Spectroscopy Analysis. *J. Alloys Compd.* **1997**, *253*, 542–546.
- (2) Millet, P.; Dantzer, P. Hydriding Kinetics Analysis by the Frequency Response Method: Application to the $\text{ZrNi}-\text{H}_2(g)$ System. *J. Alloys Compd.* **2002**, *330*, 476–482.
- (3) Millet, P. Pneumatochemical Impedance Spectroscopy. 1. Principles. *J. Phys. Chem. B* **2005**, *109*, 24016–24024.
- (4) Millet, P. Pneumatochemical Impedance Spectroscopy. 2. Dynamics of Hydrogen Sorption by Metals. *J. Phys. Chem. B* **2005**, *109*, 24025–24030.
- (5) Millet, P.; Decaux, C.; Ngameni, R.; Guymont, M. Experimental Requirements for Measuring Pneumatochemical Impedances. *Rev. Sci. Instrum.* **2007**, *78*, 123902–123902.
- (6) Millet, P.; Decaux, C.; Ngameni, R.; Guymont, M. Fourier-Domain Analysis of Hydriding Kinetics Using Pneumato-Chemical Impedance Spectroscopy. *Res. Lett. Phys. Chem.* **2007**, *2007*, 96251.
- (7) Millet, P.; Lebouin, C.; Ngameni, R.; Ranjbari, A.; Guymont, M. Hydriding Reaction of LaNi_5 : Correlations between Thermodynamic States and Sorption Kinetics during Activation. *Res. Lett. Phys. Chem.* **2008**, *2008*, 346545.
- (8) Lebouin, C.; Soldo, Y.; Grigoriev, S.; Guymont, M.; Millet, P. Kinetics of Hydrogen Sorption by Palladium Nanoparticles. *Int. J. Hydrogen Energy* **2013**, *38*, 966–972.
- (9) Kim, Y.-H.; Shin, E.-C.; Kim, S.-J.; Park, C. N.; Kim, J.; Lee, J.-S. Chemical Diffusivity for Hydrogen Storage: Pneumatochemical Intermittent Titration Technique. *J. Phys. Chem. C* **2013**, DOI: 10.1021/jp401286b, companion article.
- (10) Carman, P. C.; Haul, R. A. W. Measurement of Diffusion Coefficients. *Proc. R. Soc. London, Ser. A* **1954**, *222*, 109–118.
- (11) Crank, J. *The Mathematics of Diffusion*; Clarendon Press: Oxford, U.K., 1979.
- (12) Carslaw, H. S.; Jaeger, J. C. *Conduction of Heat in Solids*; Clarendon Press: Oxford, U.K., 1959.
- (13) Wen, C. J.; Ho, C.; Boukamp, B. A.; Raistrick, I. D.; Weppner, W.; Huggins, R. A. Use of Electrochemical Methods to Determine Chemical-Diffusion Coefficients in Alloys: Application to 'LiAl'. *Int. Mater. Rev.* **1981**, *26*, 253–268.
- (14) Weppner, W.; Huggins, R. A. Electrochemical Methods for Determining Kinetic Properties of Solids. *Annu. Rev. Mater. Sci.* **1978**, *8*, 269–311.
- (15) Huggins, R. A. *Advanced Batteries: Materials Science Aspects*; Springer: New York, 2008.
- (16) Johnson, D. *ZView: A Software Program for IES Analysis*, version 3.3, Scribner Associates Inc., Southern Pines, NC, USA 2012
- (17) *MEISP-Multiple Electrochemical Impedance Spectra Parameterization*, User Manual, version 3.0; Kumho Petrochemical R&D Center: Daejeon, South Korea, 2002.
- (18) Boukamp, B. A.; den Otter, M. W.; Bouwmeester, H. J. M. Transport Processes in Mixed Conducting Oxides: Combining Time Domain Experiments and Frequency Domain Analysis. *J. Solid State Electrochem.* **2004**, *8*, 592–598.

- (19) Millet, P.; Dantzer, P. Impedance of Metal Hydride Electrodes. Rate of Phase Transformation Limited by Nucleation and Growth Mechanisms. *Electrochim. Commun.* **1999**, *1*, 163–166.
- (20) Barsoukov, E.; Kim, J.; Kim, D.; Hwang, K.; Yoon, C.; Lee, H. Parametric Analysis Using Impedance Spectroscopy: Relationship between Material Properties and Battery Performance. *J. New Mater. Electrochem. Syst.* **2000**, *3*, 301–308.
- (21) Barsoukov, E.; Kim, D.; Lee, H.; Lee, H.; Yakovleva, M.; Gao, Y.; Engel, J. Comparison of Kinetic Properties of LiCoO_2 and $\text{LiTi}_{0.05}\text{Mg}_{0.05}\text{Ni}_{0.7}\text{Co}_{0.2}\text{O}_2$ by Impedance Spectroscopy. *Solid State Ionics* **2003**, *161*, 19–29.
- (22) Barsoukov, E.; Macdonald, J. R. *Impedance Spectroscopy: Theory, Experiment, and Applications*; Wiley InterScience: New York, 2005.
- (23) Losee, D. L. Admittance Spectroscopy of Impurity Levels in Schottky Barriers. *J. Appl. Phys.* **1975**, *46*, 2204–2212.
- (24) Bisquert, J. Beyond the Quasistatic Approximation: Impedance and Capacitance of an Exponential Distribution of Traps. *Phys. Rev. B* **2008**, *77*, 235203.
- (25) Bisquert, J. Theory of the Impedance of Electron Diffusion and Recombination in a Thin Layer. *J. Phys. Chem. B* **2002**, *106*, 325–333.
- (26) Bisquert, J.; Belmonte, G.; Santiago, F.; Ferriols, N.; Yamashita, M.; Pereira, E. Application of a Distributed Impedance Model in the Analysis of Conducting Polymer Films. *Electrochim. Commun.* **2000**, *2*, 601–605.
- (27) Bisquert, J.; Vikhrenko, V. S. Analysis of the Kinetics of Ion Intercalation. Two State Model Describing the Coupling of Solid State Ion Diffusion and Ion Binding Processes. *Electrochim. Acta* **2002**, *47*, 3977–3988.
- (28) Levi, M.; Aurbach, D. Distinction between Energetic Inhomogeneity and Geometric Non-Uniformity of Ion Insertion Electrodes Based on Complex Impedance and Complex Capacitance Analysis. *J. Phys. Chem. B* **2005**, *109*, 2763–2773.
- (29) Lee, J.-W.; Pyun, S.-I. Anomalous Behaviour of Hydrogen Extraction from Hydride-Forming Metals and Alloys under Impermeable Boundary Conditions. *Electrochim. Acta* **2005**, *50*, 1777–1805.
- (30) Shin, E.-C.; Seo, H.-H.; Kim, J.-H.; Ahn, P.-A.; Park, S. M.; Lim, Y. W.; Kim, S. J.; Kim, C. H.; Kim, D. J.; Hong, C. K.; et al. A New Diagnostic Tool for the Percolating Carbon Network in the Polymer Matrix. *Polymer* **2013**, *54*, 999–1003.
- (31) Jacobsen, T.; West, K. Diffusion Impedance in Planar, Cylindrical and Spherical Symmetry. *Electrochim. Acta* **1995**, *40*, 255–262.
- (32) Ahn, P.-A.; Shin, E.-C.; Kim, G.-R.; Lee, J.-S. Application of Generalized Transmission Line Models to Mixed Ionic-Electronic Transport Phenomena. *J. Korean Ceram. Soc.* **2011**, *48*, 549–558.
- (33) Ahn, P.-A.; Shin, E.-C.; Jo, J.-M.; Yu, J. H.; Woo, S.-K.; Lee, J.-S. Mixed Conduction in Ceramic Hydrogen/Steam Electrodes by Hebb-Wagner Polarization in the Frequency Domain. *Fuel Cells* **2012**, *12*, 1070–1084.
- (34) Johnson, H. W.; Graham, M. *High-Speed Signal Propagation: Advanced Black Magic*; Prentice Hall: New York, 2003.
- (35) Macdonald, J. R. Impedance Spectroscopy. *Ann. Biomed. Eng.* **1992**, *20*, 289–305.
- (36) Lee, J.-S.; Yoo, H.-I. Direct Measurement of Partial Ionic Conductivity of $\text{Co}_{1-\delta}\text{O}$ via Impedance Spectroscopy Combined with DC Relaxation. *Solid State Ionics* **1994**, *68*, 139–149.
- (37) Lee, J.-S.; Yoo, H.-I. A New Assessment of Ionic Conductivity of $\text{YBa}_2\text{Cu}_3\text{O}_x$ via AC Impedance Spectroscopy Combined with DC Relaxation. *J. Electrochem. Soc.* **1995**, *142*, 1169–1176.
- (38) Thompson, W. J.; Macdonald, J. R. Discrete and Integral Fourier Transforms: Analytical Examples. *Proc. Natl. Acad. Sci.* **1993**, *90*, 6904–6908.
- (39) Macdonald, J. R., Ed. *Impedance Spectroscopy: Emphasizing Solid Materials and Systems*; Wiley-Interscience: New York, 1987; pp 1–346.
- (40) Boukamp, B. A. Practical Application of the Kramers-Kronig Transformation on Impedance Measurements in Solid State Electrochemistry. *Solid State Ionics* **1993**, *62*, 131–141.
- (41) Boukamp, B. A Linear Kronig-Kramers Transform Test for Immittance Data Validation. *J. Electrochem. Soc.* **1995**, *142*, 1885–1994.
- (42) Park, C.-N.; Lee, J.-Y. Kinetic Properties of the Hydrogenation of the FeTi Intermetallic Compound. *J. Less-Common Met.* **1983**, *91*, 189–201.